Atmos. Chem. Phys., 10, 4187–4206, 2010
www.atmos-chem-phys.net/10/4187/2010/
doi:10.5194/acp-10-4187-2010

Atmospheric Chemistry and Physics

NO_3 radical measurements in a polluted marine environment: links to ozone formation

R. McLaren[1], P. Wojtal[1], D. Majonis[1], J. McCourt[1], J. D. Halla[1], and J. Brook[2]

[1]Centre for Atmospheric Chemistry, York University, North York, ON, Canada
[2]Air Quality Research Division, Environment Canada, Toronto, ON, Canada

Received: 20 October 2009 – Published in Atmos. Chem. Phys. Discuss.: 18 November 2009
Revised: 9 April 2010 – Accepted: 19 April 2010 – Published: 5 May 2010

Abstract. Nighttime chemistry in polluted regions is dominated by the nitrate radical (NO_3) including its direct reaction with natural and anthropogenic hydrocarbons, its reaction with NO_2 to form N_2O_5, and subsequent reactions of N_2O_5 to form HNO_3 and chlorine containing photolabile species. We report nighttime measurements of NO_3, NO_2, and O_3, in the polluted marine boundary layer southwest of Vancouver, BC during a three week study in the summer of 2005. The concentration of N_2O_5 was calculated using the well known equilibrium, NO_3+$NO_2 \rightleftharpoons N_2O_5$. Median overnight mixing ratios of NO_3, N_2O_5 and NO_2 were 10.3 ppt, 122 ppt and 8.3 ppb with median N_2O_5/NO_3 molar ratios of 13.1 and median nocturnal partitioning of 4.9%. Due to the high levels of NO_2 that can inhibit approach to steady-state, we use a method for calculating NO_3 lifetimes that does not assume the steady-state approximation. Median and average lifetimes of NO_3 in the NO_3-N_2O_5 nighttime reservoir were 1.1–2.3 min. We have determined nocturnal profiles of the pseudo first order loss coefficient of NO_3 and the first order loss coefficients of N_2O_5 by regression of the NO_3 inverse lifetimes with the $[N_2O_5]/[NO_3]$ ratio. Direct losses of NO_3 are highest early in the night, tapering off as the night proceeds. The magnitude of the first order loss coefficient of N_2O_5 is consistent with, but not verification of, recommended homogeneous rate coefficients for reaction of N_2O_5 with water vapor early in the night, but increases significantly in the latter part of the night when relative humidity increases beyond 75%, consistent with heterogeneous reactions of N_2O_5 with aerosols with a rate constant $k_{het} = (1.2 \pm 0.4) \times 10^{-3}\,s^{-1} - (1.6 \pm 0.4) \times 10^{-3}\,s^{-1}$. Analysis indicates that a correlation exists between overnight integrated N_2O_5 concentrations in the marine boundary layer, a surrogate for the accumulation of chlorine containing photolabile species, and maximum 1-h average O_3 at stations in the Lower Fraser Valley the next day when there is clear evidence of a sea breeze transporting marine air into the valley. The range of maximum 1-h average O_3 increase attributable to the correlation is $\Delta O_3 = +1.1$ to $+8.3$ ppb throughout the study for the average of 20 stations, although higher increases are seen for stations far downwind of the coastal urban area. The correlation is still statistically significant on the second day after a nighttime accumulation, but with a different spatial pattern favouring increased O_3 at the coastal urban stations, consistent with transport of polluted air back to the coast.

Correspondence to: R. McLaren
(rmclaren@yorku.ca)

1 Introduction

It has long been recognized that radicals are important initiators of chemical reactions in the atmosphere. While the hydroxyl radical (OH) dominates the daytime chemistry of both clean and polluted atmospheres (Finlayson-Pitts and Pitts, 2000), the nitrate radical (NO_3) is found to be an important radical initiator and intermediate in the conversion of NO_x (NO+NO_2) to nitric acid (HNO_3). The first measurements of NO_3 in the polluted troposphere were made by differential optical absorption spectroscopy (DOAS) in continental North America with levels greater than 300 ppt observed one hour after sunset (Platt et al., 1980; Noxon et al., 1980). Since then, many studies have demonstrated the importance of NO_3 at far lower levels. In general, NO_3 is less reactive than OH in its reaction with volatile organic compounds (VOCs), although there are several important species for which NO_3 is a competing or dominant sink compared to

other initiators. For example, in the marine boundary layer (MBL) of the North Atlantic, it has been shown that NO_3 is a more efficient sink for dimethyl sulphide (DMS) at night than OH is during the day (Allan et al., 2000). In the continental boundary layer of Europe, it was found that the relative 24-h average contribution of NO_3-initiated oxidation of all VOCs was 28%, compared to 55% for OH and 17% for O_3 (Geyer et al., 2001). In the Northeast US, it was found that approximately 20% of isoprene, the single largest VOC emission to the atmosphere on a global scale, is oxidized by NO_3 at night despite its dominant emission during the day, and that secondary organic aerosol mass derived from NO_3-initiated isoprene oxidation at night exceeded that initiated by OH by 50% (Brown et al., 2009).

It is well known that NO_3 reacts reversibly with NO_2 to form dinitrogen pentoxide (N_2O_5), and that the hydrolysis of N_2O_5 on aerosols is an important global pathway for the conversion of NO_x to nitric acid (HNO_3) (Dentener and Crutzen, 1993). It has also been known for some time that N_2O_5 can react with sea salt to form $ClNO_2$ (Finlayson-Pitts et al., 1989). Recent observations of high levels of $ClNO_2$ at night exceeding 1 ppb in the marine boundary layer were linked to N_2O_5 reactions (Osthoff et al., 2008). Recent observations of Cl_2 in the marine boundary layer at levels up to 150 ppt (Spicer et al., 1998; Finley and Saltzman, 2006) have several possible mechanistic sources including a daytime photolytic source involving a surface mediated reaction of OH on sea salt aerosols (Knipping et al., 2000), dark reactions of $ClONO_2$ with NaCl (Finlayson-Pitts et al., 1989), and more recently, the production of Cl_2 arising from N_2O_5 reactions on acidic aerosols through the $ClNO_2$ intermediate (Roberts et al., 2008). Studies have also shown that N_2O_5 and NO_2 can react heterogeneously with HCl on surfaces to produce $ClNO_2$ and ClNO respectively (Raff et al., 2009). All three of the previously mentioned chlorine species, $ClNO_2$, Cl_2 and ClNO, are photolabile and capable of accumulating overnight. Upon photolysis during the day, these photolabile species will release Cl radicals that are very reactive with many trace gases. Several recent modelling studies have suggested that the release of Cl radicals from these photolabile species can contribute to enhanced O_3 formation in coastal urban regions (Knipping and Dabdub, 2003; Finley and Saltzman, 2006; Osthoff et al., 2008; Simon et al., 2009; Raff et al., 2009).

The Lower Fraser Valley (LFV), straddling the Canada/USA border in western North America and containing the city of Vancouver, is an example of a coastal urban area. The meteorology and air quality in the LFV is complicated by the influence of surrounding mountains and the Pacific Ocean to the west. The valley has been the subject of major field studies (Steyn et al., 1997; Li, 2004) and modeling studies (Hedley et al., 1997; Hedley et al., 1998) whose objectives were to further our understanding of O_3 and aerosol formation and transport in the region. A common transport scenario that can often be seen in multiple day smog episodes in the region is: (i) sea breezes carrying urban emissions into the valley, (ii) outflow of polluted air via land breezes at night into the MBL, (iii) stagnation of polluted air in the MBL overnight, and iv) transport of the overnight processed air back into the valley the next day via sea breezes again. The stagnation effect in the Strait has been noted previously and has been described as the wake induced stagnation effect (Brook et al., 2004). The nocturnal chemistry that may be occurring in the Strait has not been previously addressed.

In this paper, we describe our analysis of data collected during a limited "scoping study" that took place for 3 weeks in the summer of 2005. The primary purpose of the study was to measure nighttime NO_3 and NO_2 and to determine the levels of N_2O_5 in the MBL at a suitable location in the Strait of Georgia where nighttime pooling of pollutants may occur, in order to assess the role of nighttime chemistry, halogen activation and its link to air quality in the LFV. The study was also supported by daytime measurements of various trace gases by multiple-axis DOAS (MAX-DOAS), which will not be discussed here.

2 Nighttime chemistry

Important reactions involved in the formation and loss of NO_3 and N_2O_5 are shown below.

$$NO_2 + O_3 \rightarrow NO_3 + O_2 \qquad k_1 \tag{R1}$$

$$NO_3 + NO_2 + M \rightarrow N_2O_5 + M \qquad k_{2f} \tag{R2f}$$

$$N_2O_5 + M \rightarrow NO_3 + NO_2 + M \qquad k_{2r} \tag{R2r}$$

$$NO_3 + h\nu \rightarrow NO_2 + O(^3P) \qquad J_{NO_{3a}} \tag{R3a}$$

$$\rightarrow NO + O_2 \qquad J_{NO_{3b}} \tag{R3b}$$

$$NO_3 + NO \rightarrow 2NO_2 \qquad k_4 \tag{R4}$$

$$NO + O_3 \rightarrow NO_2 + O_2 \qquad k_5 \tag{R5}$$

$$NO + RO_2^{\cdot} \rightarrow NO_2 + RO^{\cdot} \qquad k_6 \tag{R6}$$

$$NO_3 + VOC \rightarrow \text{other} \qquad k_7 \tag{R7}$$

$$NO_3 + DMS \rightarrow \text{products} \qquad k_8 \tag{R8}$$

$$N_2O_5 + H_2O_{(p)} \rightarrow 2HNO_{3(p,g)} \qquad k_9 \tag{R9}$$

$$N_2O_5 + H_2O_{(g)} \rightarrow 2HNO_{3(g)} \qquad k_{10} \tag{R10}$$

$$N_2O_5 + NaCl_{(s,aq)} \rightarrow ClNO_{2(g,aq)} + NaNO_{3(s,aq)} \qquad k_{11} \tag{R11}$$

$$ClNO_{2(aq)} + H^+_{(aq)} \rightarrow ClNO_2H^+_{(aq)} \tag{R12a}$$

$$ClNO_2H^+_{(aq)} + Cl^-_{(aq)} \rightarrow Cl_{2(g)} + HNO_{2(aq)} \tag{R12b}$$

$$ClNO_2 + h\nu \rightarrow Cl^{\cdot} + NO_2 \qquad J_{ClNO_2} \tag{R13}$$

$$Cl_2 + h\nu \rightarrow 2Cl^{\cdot} \qquad J_{Cl2} \qquad \text{(R14)}$$

NO_3 is initially formed from the reaction of NO_2 with O_3 (Reaction R1). During the daytime, NO_3 rapidly photolyzes (Reaction R3) via two channels at wavelengths less than 640 nm. Channel (Reaction R3a) is dominant, giving rise to a daytime lifetime of NO_3 of several seconds at solar noon (Orlando et al., 1993) and ultimately resulting in low levels of NO_3 during the daytime, typically less than a few ppt (Platt et al., 1980). Reaction of NO_3 with NO (Reaction R4) is also fast. Since NO_x ($NO+NO_2$) from combustion sources is primarily emitted as NO (>90% typically), NO_3 losses from this reaction will be large close to these sources, although the NO can also react quickly with O_3 (Reaction R5) or peroxy radicals (R6) to produce NO_2. At typical background levels of O_3 in the troposphere (40 ppb), the lifetime of NO due to reaction with O_3 is 56 seconds at 298K. NO will be quantitatively (>99%) converted to NO_2 in 3-5 minutes at this rate, provided that the emission of NO does not consume the O_3. Other direct losses of NO_3 include abstraction and addition reactions with VOCs (Reaction R7). Such reactions can yield oxygenated organic products that are condensable on particles (McLaren et al., 2004). The reactions of NO_3 with VOCs are generally slower than equivalent reactions with the hydroxyl radical (OH) or atomic chlorine (Cl), although certain reactions are extremely fast, including reactions with alkenes, cresols, isoprene (Brown et al., 2009), monoterpenes (Wängberg et al., 1997a) and dimethylsulphide (Reaction R8), the last being naturally emitted from oceanic biota.

Another significant loss mechanism for NO_3 is the reversible 3-body formation of dinitrogen pentoxide, N_2O_5 (Reaction R2). This reaction is reversible because of the thermal decomposition of N_2O_5 (Reaction R2), yielding a highly temperature dependent equilibrium between NO_3, NO_2, and N_2O_5 (Wängberg et al., 1997b). The temperature equilibrium constant is given by:

$$K_{eq}(T) = k_{2f}(T)/k_{2r}(T) = [N_2O_5]/[NO_3][NO_2] \qquad (1)$$

The equilibrium is favoured to the right under conditions of high NO_2, allowing a buildup of significant levels of N_2O_5, which can act as a nighttime reservoir of NO_x. Because an equilibrium exists (Reactions R2f, R2r), direct losses of N_2O_5 are also indirect losses of NO_3. These indirect losses of NO_3 include heterogeneous reactions of N_2O_5 on moist particles to form nitric acid and particle nitrate (Reaction R9) and homogeneous reaction with water to form gaseous nitric acid (Reaction R10). Nitric acid is lost due to multiple processes including dry and wet deposition, photolysis, and reaction with NH_3 to form particulate ammonium nitrate.

It was shown some time ago that both N_2O_5 and $ClONO_2$ can react individually with NaCl(s) to form nitryl chloride, $ClNO_2$ (Reaction R11) and molecular chlorine, Cl_2, respectively (Finlayson-Pitts et al., 1989). The exact mechanism for production of Cl_2 in coastal areas is the subject of intense research at this time. It was recently shown by Roberts et al. (2008) that N_2O_5 can oxidize Cl^- to Cl_2 in acidic aerosols through acid assisted reaction of the $ClNO_2$ intermediate with Cl^-, and they have proposed a two step mechanism (Reactions R12a, R12b). Both products, $ClNO_2$ and Cl_2, are chlorine atom precursors that can photolyze at sunrise to generate the reactive chlorine atom (Reactions R13, R14). The chlorine atoms in turn can contribute to ozone formation through their reaction with VOCs (Finlayson-Pitts, 2003).

Fig. 1. Map of the Lower Fraser Valley and surrounding marine areas. Solid squares indicate Greater Vancouver Regional District air quality monitoring stations. Circles with cross indicate Environment Canada climate stations. The inset shows the measurement site at East Point, Saturna Island.

3 Experimental

3.1 Location

The map in Fig. 1 indicates the location of the study. Instrumentation was located at East Point, Saturna Island. Saturna Island is one of the Gulf Islands in the Strait of Georgia, situated at the confluence of the northwest-southeast and northeast-southwest arms of the Strait. The identity, distance and direction to major urban areas from the measurement site include Vancouver BC, 55 km NNW; Victoria BC, 46 km SSW; Bellingham WA, 41 km E; and Seattle WA, 142 km SSE (not shown). The mainland in the LFV is 20 km east of the site across the Strait. The island is situated in the midst of major international shipping channels that lead to the Strait of Juan de Fuca, and the open Pacific Ocean. Instrumentation was located on a grassy patch next to the ocean at an elevation of 23 m a.s.l. There are very few direct anthropogenic sources on the island, especially at the eastern tip, although the site is directly influenced by marine vessel traffic.

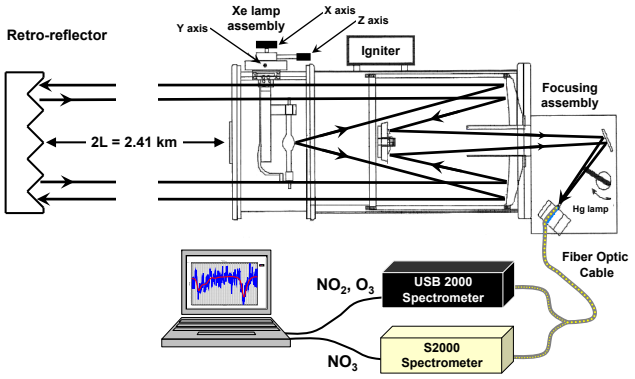

Fig. 2. Instrumental setup of the DOAS system.

An Environment Canada weather station is located at East Point, at the location of the DOAS telescope (48°47.034′ N Longitude: 123°2.685′ W). The meteorological observations were taken at a height of 24.4 m a.s.l. Meteorological data were obtained from the National Climate Data Archive (Environment Canada, 2008). Also located on the Island is a Canadian Air and Precipitation Monitoring (CAPMon) network station operated by Environment Canada. The NO_2 measured at this station was performed with a chemiluminescence (NO_x) instrument retrofit with a photolytic converter, for measurement of "true" NO_2. The station is located 6 km west of the East Point location at an altitude of 200 m a.s.l. on the south side of the island. The maximum elevation of Saturna Island is 400 m a.s.l. The Gulf islands are moderately contoured and can act as barriers to surface air flow in the marine layer. Measurements were made from 23 July–9 August 2005. Sunset and sunrise times at this location during the period were 08:51 p.m. (±11 min) and 5:46 a.m. (±11 min) respectively.

The Greater Vancouver Regional District (GVRD) operates a network of air quality monitoring stations (19 stations in 2005) throughout the LFV with continuous observations of O_3, NO_x and other pollutants using standard instrumentation and methodologies. In particular, the NO_x instruments are standard chemiluminescence instruments with Mo converters. As such, the reported NO_2 is a maximum estimate as it may contain some oxidized NO_y components. This artifact is less significant for the more urban stations where we expect NO_y is >90% NO_x ($NO+NO_2$). The locations of the stations in the network are shown in Fig. 1. Hourly average data from the network was provided by the GVRD.

3.2 DOAS measurements

DOAS measurements were made using a modified DOAS 2000 Instrument (TEI Inc.), Fig. 2. The instrument utilizes a 150 W high pressure Xe-arc lamp and a coaxial Cassegrain telescope. The outgoing beam is collimated by the outer portion of the 8″ primary telescope mirror. The beam traverses through the open atmosphere and is reflected from a retro reflector composed of $7\times2''$ corner cube reflectors. The DOAS retro reflector was located on Tumbo Island (Fig. 1 inset) at an elevation of 6 m a.s.l. The total path length was 2.407 km with the majority of the path (2.1 km) over the ocean at a mean elevation of 15 m a.s.l. The return beam is focused by the inner portion of the primary mirror onto a modified detector system including a bifurcated quartz fiber optic (Ocean Optics) with dual 400 µm fibers, each fiber leading to a different fiber optic spectrometer. One spectrometer was optimized for NO_2 and UV absorption features (USB2000, Grating #10, 295–492 nm, 1800 lines mm^{-1}, 2048 element CCD, 25 µm slit, UV2 upgrade, L2 lens) with optical resolution of ∼ 0.5 nm; and one was optimized for NO_3 absorption in the red end of the visible spectrum (S2000, λ_{blaze} =750 nm, 550–835 nm, 1200 lines mm^{-1}, 2048 element CCD, 25 µm slit, L2 lens) with an optical resolution of ∼0.6 nm. A small diffuser was installed in the entrance end of the fiber to lower atmospheric turbulence noise (Stutz and Platt, 1997). The spectrometers were cooled to −5 °C in a portable freezer.

For the NO_3 measurements (S2000), data was collected with OOIBase32 software. Typical integration times were 25–30 ms. Averages of 30 000 spectra were computed and streamed to disk, resulting in a time resolution of ca 8–15 min when visibility was good. For the NO_2 measurements (USB2000), custom acquisition software was written in LabView to acquire spectra with typical integration times of 200–300 ms, and 2500 averages for spectra with a time resolution of 8–12 min. Mercury lamp reference spectra were collected periodically for wavelength calibration and for convoluting molecular reference spectra to the slit function of the spectrometer. Xenon lamp spectra were collected for use in fitting to the measured spectra. Each ambient spectrum was also corrected for electronic offset and dark noise.

The averaged spectra were fit using DOASIS software (Kraus, 2006). For NO_3, typical fit scenarios included a convoluted NO_3 reference spectrum at 298 K (Yokelson et al., 1994), a convoluted water spectrum (Coheur et al., 2002), a Xe lamp spectrum in the region from 617–673 nm and a third order polynomial. The NO_3 mixing ratios were not corrected for the temperature dependence of the NO_3 cross section (Osthoff et al., 2007), although the change in the peak cross section of NO_3 at 662 nm over the temperature range of this study varies by only ±1.9%. It was found that better results were generally obtained by using an early evening or early morning ambient spectrum, at a time when NO_3 is determined to be negligible, in place of a lamp reference spectrum (Platt, 1994). The presence of two strong absorption features at 623 and 662 nm were used to qualitatively identify the presence of NO_3. For NO_2, fit scenarios included a lamp reference spectrum, a convoluted spectrum of NO_2 (Voigt et al., 2002) in the region from 422–437.5 nm and a third order polynomial. Independent studies using injections of high concentrations of a standard mixture of NO_2 in air into an absorption cell positioned in the DOAS beam path

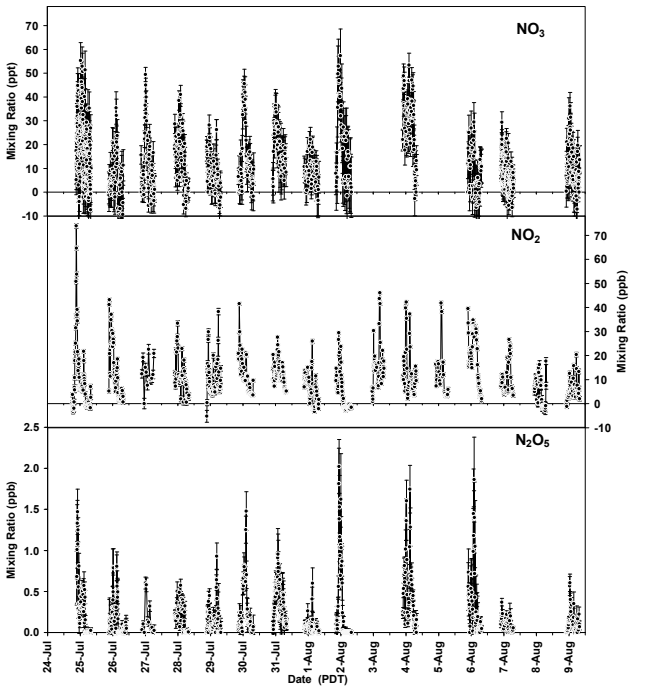

Fig. 3. Observations of NO_3 and NO_2 and calculated N_2O_5 at East Point, 2005.

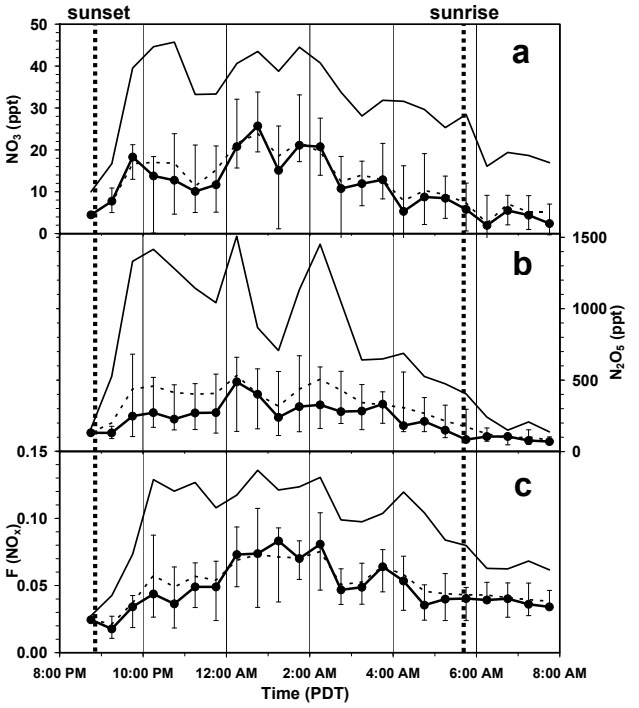

Fig. 4. Study average nocturnal variation in **(a)** NO_3 **(b)** N_2O_5 and **(c)** $F(NO_x)$ – partitioning of nitrogen in nighttime reservoir species (see Eq. 2) Shown are the average (dotted line), median (solid point), 95th (solid line), 75th (top whisker) and 25th percentiles (bottom whisker) in each 30 min time bin.

confirmed that our DOASIS retrieval methods were accurate to within 10% for NO_2 mixing ratios from 1–100 ppb. Detection limits for NO_3 and NO_2 were 4 ppt and 2 ppb respectively, taken as 2σ in the residuals of the fit.

Ozone was also measured by DOAS by fitting the nighttime spectra collected with the UV spectrometer in the region of 316.8–329.9 nm. The fit included a reference spectrum for O_3 (Bogumil et al., 2001), one for NO_2, a Xe lamp spectrum and third order polynomial. This region is not the ideal region for measurement of O_3 by DOAS, as the differential absorption cross sections are relatively small. Despite this, O_3 was measurable with uncertainties of ± 5 ppb simultaneously in the same path as NO_2 and NO_3. This O_3 data set was preferred compared to the use of the O_3 measurements from the CAPMon station 6 km away due to the observation of differences in NO_2 pollutant levels on the north and south sides of the island. Overall the average nighttime O_3 levels at East Point were 5.5 ppb lower than those measured at the CAPMon station.

4 Results and discussion

4.1 NO_3, NO_2 and O_3 observations

Observations of NO_3 and NO_2 throughout the study are shown in Fig. 3. Measurements were made on 16 nights for NO_2 and O_3, and 13 nights for NO_3. Negative results are shown for completeness, and are expected to occur when levels are at, or below the detection limit. A summary of statistics for the chemical observations of NO_3, NO_2 and O_3 at night (between 8:00 p.m. and 8:00 a.m. PLT) are given in Table 1, along with other important meteorological observations that are relevant for formation and loss of NO_3 and N_2O_5. Maximum mixing ratios of NO_3 (8–15 min average) were above 20 ppt every night. The range of nightly maximum levels was 22–57 ppt, with an average nightly maximum level of 40.0 ppt, roughly consistent with the 95th percentile of all observations of 38.4 ppt. The average and median for all nighttime observations of NO_3 were 13.1 ppt and 10.2 ppt, respectively. Measurements of NO_3 were not made during the day as they are generally below the detection limit. Thus, median and average NO_3 mixing ratios relevant for 24 h periods would be approximately half the values stated above, 5.1–6.5 ppt.

A nocturnal profile for NO_3, based on 30 min time bins of all observations, is given in Fig. 4. The profile shows mixing ratios of NO_3 increasing after sunset with a maximum between midnight and 1 am (25th, 50th, 75th percentiles and average). NO_3 slowly decays after that time until sunrise, when it approaches zero. The central values and range of concentrations we report here are similar to values reported in summer time in other marine areas (Vrekoussis et al., 2007). Despite the higher NO_2 levels in this region that

Table 1. Statistics for nighttime measurements at East Point (8:00 p.m.–8:00 a.m. PDT).

	Max	95%	75%	Average	Median	25%	Min	N
NO_3 (ppt)	57.3	38.4	20.7	13.1	10.2	3.8	<DL	952
NO_2 (ppb)	74.0	30.7	14.5	10.3	8.3	3.5	<DL	810
N_2O_5 (ppt)	2022	912	331	244	122	23.2	<DL	678
O_3 (ppb)	84.6	60.3	37.5	29.2	24.9	18.8	<DL	528
$\tau^q_{NO_3}$ (sec)[a]	2624	503	135	139	66	26	<DL	452
$\tau_S NO_3$ (sec)[a]	1607	368	160	129	84	39	6	452
$F(NO_x)$[a,b]	0.201	0.122	0.075	0.056	0.049	0.030	0.009	452
T (^oC)[c]	24.6	22.1	19.8	18.3	18.0	16.5	14.4	192
RH (%)[c]	90	86	82	76	79	71	50	192
H_2O (%)[c]	1.94	1.82	1.66	1.56	1.56	1.47	1.21	192
WS (km hr^{-1})[c]	30.0	20.9	17.0	11.1	11.0	6.0	0	192

[a] $\tau^q_{NO_3}$ (Eq. 13), τ_S NO_3 (Eq. 3), and $F(NO_x)$ (Eq. 2) were calculated only when NO_2 >2 ppb and NO_3 >4 ppt. [b] $F(NO_x) = [NO_3] + 2\times[N_2O_5]/[NO_2]+[NO_3]+2\times[N_2O_5]$. [c] Hourly averages.

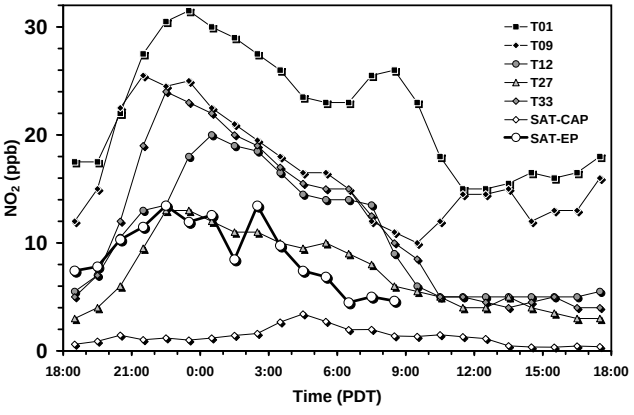

Fig. 5. Comparison of NO_2 diurnal profiles at Saturna Island, East Point (SAT-EP) versus the Saturna CAPMon station (SAT-CAP) and other LFV monitoring stations (refer to Fig. 1). Hourly average mixing ratios are shown. Statistical ranges are not shown for clarity.

would increase the production rate of NO_3 via R1, the levels of NO_3 are not necessarily higher than seen in other less polluted areas. This is due to the subsequent loss of NO_3 to form N_2O_5 via reaction (Reaction R2f), also proportional to NO_2, rendering NO_3 insensitive to NO_2 as a first approximation.

Nighttime ozone levels were generally low at East Point, with median values of 24.9 ppb, marginally less than the 30.4 ppb observed at the CAPMon station. Despite this, the nighttime median ozone levels at East Point were significantly higher than those observed at all monitoring stations in the LFV mainland, where the range was 1.0–18.5 ppb for 19 stations. Frequent titrations of ozone to zero are observed at the mainland stations at night, due to a combination of anthropogenic emissions of NO_x from on-road vehicles in a shallow nocturnal inversion layer, and high rates of deposition over continental surfaces. Deposition velocities of ozone over water are known to be significantly smaller.

Nighttime levels of NO_2 at East Point were quite high for the MBL, as indicated in Fig. 3 and Table 1. Median and average nighttime levels were 8.3 ppb and 10.3 ppb respectively. These levels of NO_2 are much higher than those reported in many recent studies of nighttime chemistry in the MBL (Allan et al., 2000; Martinez et al., 2000; Vrekoussis et al., 2004; Matsumoto et al., 2006; Vrekoussis et al., 2007). Although vehicular traffic is minimal on the island, the proximity of Saturna Island to multiple populated regions gives rise to an overall elevated background level of NO_x in this marine region. Nocturnal build up of pollutants can occur in the Strait during stagnation events, due to the wake induced stagnation effect (Brook et al., 2004). In addition, marine vessels are a major contributor to the total emissions of NO_x in the region, especially in the Strait of Georgia. A recent air pollutant emissions inventory of the LFV (Metro Vancouver, 2007), including mainland and marine regions, indicated that emissions of NO_x from marine vessels were 8.4×10^6 kg yr^{-1} in 2005 or 14% of the total anthropogenic NO_x emissions, and are projected to rise in both absolute and relative terms to 13.6×10^6 kg yr^{-1}, and 30% respectively, by the year 2030. Most of these emissions are in the MBL in the western end of the domain (Fig. 1). Marine vessels destined for the Pacific Ocean leave Vancouver ports travelling south and generally follow a shipping lane that follows the Canada/USA border leading to the Strait of Juan de Fuca. This brings ocean going vessels to within a few kilometers of East Point, frequently visible throughout the study.

A comparison of the study average nocturnal pattern of NO_2 measured by DOAS, compared to that reported at a few representative monitoring stations in the LFV is shown in Fig. 5. The mixing ratios of NO_2 at Saturna are on the lower end of the range observed in the Valley. The highest NO_2

levels are observed in the north western portion of the valley, close to the urban region of Vancouver. Station T1, in downtown Vancouver, experiences the highest NO_2 levels of all 19 reporting stations. The levels of NO_2 at East Point are similar to those seen at Station T27 (Langley, BC), a mid valley station 40 km away, 20 km inland from the coast. The nocturnal profile of NO_2 at East Point shows maximum levels in the middle of the night, as do all stations in the valley, typical of continental urban areas. The mainland stations show early morning peaks typical of vehicular traffic that is absent in the East Point profile, confirming the absence of significant vehicular traffic at the site.

The levels of NO_2 measured at East Point were clearly much higher than those simultaneously measured at the CAPMon station on Saturna Island, separated by only 6 km (Fig. 5). There are several explanations for this. First, the East Point site is more representative of the conditions experienced in the marine MBL, being at the confluence of two main stretches of the Strait at the north east tip of the island. The Gulf Islands can act as a physical barrier to surface flow and as such, emissions from marine vessels within the Strait and outflow (land breezes) from the LFV at night are likely confined to the Strait. Evidence for this lies within Fig. 6c, which shows the frequency of wind directions observed at night when winds were not stagnant ($>2\,km\,h^{-1}$). There are two main wind sectors observed at East Point at night. The first is a 50° sector from 195–245°, which collectively accounts for 67% of all nighttime observations; here within referred to as the southwest sector. The second sector, the northwest sector, from 285–335°, accounts for 18% of observations. Collectively, these two sectors account for 85% of all non-stagnant observations, and are aligned with the main directions of the channels of the Strait of Georgia; NW-SE and SW-NE. The NW sector likely contains outflow emissions from Vancouver (Hedley and Singleton, 1997) as well as marine vessel emissions, whereas the SW sector likely contains emissions from Victoria as well as marine vessel emissions. Stagnant conditions were observed 2.6% of the time.

A second reason for the low NO_2 observations at CAPMon versus East Point is related to the differences in site location, including positioning over land or water and elevation. The CAPMon site is positioned inland at an elevation of 200±5 m a.s.l. At night, the site is likely within a surface layer or nocturnal boundary layer (Brown et al., 2007) that is isolated and decoupled from the surrounding MBL. With few surface sources on the island, the NO_2 levels are low. Winds from the southwest sector approaching the CAPMon site encounter a physical barrier, a 400 m cliff at the west end of the island gradually decreasing to 250 m directly south of the CAPMon site. This physical barrier perturbs surface marine flow, as mentioned previously, and likely further decouples the CAPMon site from surface emissions at night. In contrast, the East Point site has a measurement beam elevation of 15±9 m a.s.l. situated largely within the MBL. It is exposed to surface emissions within the MBL. In addition, vertical mixing over water in the MBL will be slow, especially at night, and thus surface emissions over the water are likely stratified.

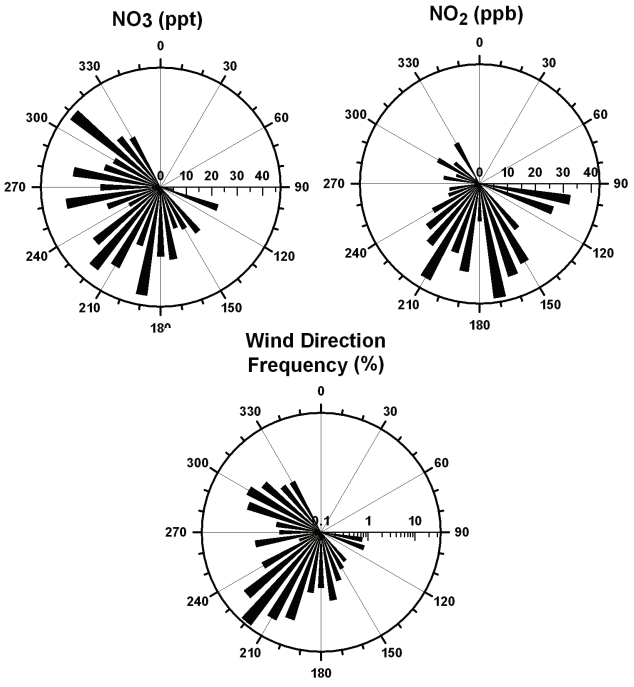

Fig. 6. Chemical and wind rose plots for **(a)** NO_3 mixing ratio **(b)** NO_2 mixing ratio and **(c)** frequency of winds, vs. wind direction. For all three plots, only data with coincident wind speeds $>2\,km\,h^{-1}$ was included. For (a) and (b) radial direction represents the 95th percentile of the group of observations in each 10° bin. Note the log scale for panel (c).

Figure 6 shows the dependence of the NO_3 and NO_2 observations on wind direction. In general NO_3 showed slightly elevated levels in the SW and NW sectors compared to the other observations. NO_2 showed elevated levels when winds were from the SE quadrant, however infrequently (7.3% of the time), and from the SW sector. It is worth noting that the SE quadrant is the quadrant that contains the closest approach of marine vessels to the tip of East Point, whereas the SW sector aligns with the shipping highways in the lower leg of the Strait of Georgia, Haro Strait, and the City of Victoria.

For the above reasons, we conclude that the site at East Point is representative of a polluted MBL at night that is frequently impacted by emissions from marine vessels and from regional anthropogenic emissions from surrounding urban areas. The NO_2 levels seen at night are similar to those observed in the less populated region of the LFV.

4.2 N_2O_5 and nighttime partitioning

N_2O_5 was calculated on a sample by sample basis from the known concentrations of NO_2 and NO_3, along with use of

the temperature dependent forward (Reaction R2f) and reverse rate constants (Reaction R2r) taken from recent recommendations (Atkinson et al., 2004). Temperature data from the meteorological database was used for each coincident observation. Uncertainties in the N_2O_5 levels have been calculated via propagation of uncertainties in the NO_3 and NO_2 values. There are also uncertainties in the forward and reverse rate constants, and hence, the corresponding equilibrium constant, K. Including a 20% uncertainty in the calculated value of the equilibrium constant, K$= k_{2f}/k_{2r}$ (Wängberg et al., 1997b), the overall relative uncertainty in the calculated N_2O_5 levels for a single point is ±28% at levels corresponding to the 95th percentile (∼900 ppt). In calculating N_2O_5, the assumption is that equilibrium exists between NO_2, NO_3 and N_2O_5. This is generally true under conditions of high temperatures and high NO_2 that promote high turnover times of NO_3 and N_2O_5 for Reactions (R2f) and (R2r) respectively. For example, using the median overnight temperature of 18 °C, $k_{2r} = 1.89 \times 10^{-2}\,s^{-1}$, giving a N_2O_5 lifetime with respect to thermal decomposition of 53 seconds. Correspondingly, at the same temperature, $k_{2f} = 1.3 \times 10^{-12}\,cm^3\,molec^{-1}\,s^{-1}$, and in the presence of 8.3 ppb of NO_2 (median level), the lifetime of NO_3 with respect to reaction with NO_2 is 4 s. Thus, equilibrium is established very rapidly under these conditions. An additional uncertainty in the calculated N_2O_5 exists if the NO_3 and NO_2 are not homogeneously distributed along the light path.

Calculated N_2O_5 mixing ratios had maximum values above 300 ppt every night, ranging from 369–2022 ppt with a median maximum nightly value of 928 ppt, roughly consistent with the 95th percentile of all nighttime observations of 912 ppt. Average and median levels over the course of the night were 244 ppt and 122 ppt respectively. These levels are much higher than typically reported for the summer MBL (Allan et al., 2000; Vrekoussis et al., 2004; Matsumoto et al., 2006; Vrekoussis et al., 2007), due to the focus of other studies on less polluted locations. On the edge of the Baltic Sea in summer, the occasional N_2O_5 level up to 2 ppb during pollution events was reported (Heintz et al., 1996). N_2O_5 levels of 1 ppb were reported in moderately polluted air off the east coast of the USA, with average N_2O_5 nighttime levels of 84 ppt in the presence of average NO_2 levels of 4 ppb (Brown et al., 2004). And in the coastal area of Houston, N_2O_5 in the MBL was reported in excess of 700 ppt when NO_y was approaching 20 ppb (Osthoff et al., 2008). In the present study, the levels of N_2O_5 are much higher than the levels of NO_3, with mean and median values of the N_2O_5/NO_3 ratio of 16.8 and 13.1 respectively. This high ratio is a direct consequence of the high levels of NO_2. An important consequence of high N_2O_5/NO_3 ratios in polluted air is the potential for increased importance of indirect losses of NO_3, via reactions of N_2O_5. This rationale was noted previously (Martinez et al., 2000), and is supported by conclusions in a study of the remote MBL, namely that in remote marine air, losses of NO_3 were dominated by direct reactions with DMS, whereas in moderately polluted air, indirect losses of NO_3 via N_2O_5 reactions usually dominated (Allan et al., 2000).

Apart from the $[N_2O_5]/[NO_3]$ ratio, an additional diagnostic parameter is the molar partitioning of total oxidized nitrogen, NO_y, that is attributable to nighttime reservoir species, NO_3 and N_2O_5 (Brown et al., 2003b; McLaren et al., 2004). A similar diagnostic is the nocturnal partitioning, $F(NO_x)$, among the three equilibrium species in Reaction (R2),

$$F(NO_x) = \frac{[NO_3] + 2[N_2O_5]}{[NO_2] + [NO_3] + 2[N_2O_5]} \quad (2)$$

$F(NO_x)$ is a measure of the proportion of nitrogen oxide stored in the nocturnal reservoir of NO_3 and N_2O_5 (Brown et al., 2007). High values of $F(NO_x)$ can be indicative of long lifetimes for NO_3 and N_2O_5 and are expected to increase as temperature decreases, whereas low values of nocturnal partitioning are expected when lifetimes of NO_3 and N_2O_5 are small. In the current study, the values for $F(NO_x)$ ranged from zero to 20% with average and median values of about 5%, Table 1. These are comparable to nocturnal partitioning of 5%, calculated from data within the report of the moderately polluted summer MBL (Brown et al., 2004). The average nocturnal partitioning of 5% in the current study is also consistent with a recent report (Brown et al., 2007) in which $F(NO_x)$ was less than 10% in the continental nocturnal boundary layer, where short NO_3 lifetimes suggested rapid sinks for NO_3 and N_2O_5, but $F(NO_x)$ increased rapidly with height above the nocturnal boundary layer to 35%, coincident with a rapid increase in the NO_3 lifetime with height.

4.3 Lifetime and losses of NO_3

4.3.1 Theoretical aspects

A useful parameter to calculate is the lifetime of the NO_3 radical, τ_{NO_3}. An expression for the apparent lifetime of NO_3 can be derived with knowledge of the known source Reaction (R1), its reversible reaction to form N_2O_5 (Reactions R2f, R2r), and indeterminate losses of NO_3 and N_2O_5 such as those shown previously (e.g. Reactions R7–R11). The derivation has been presented previously (Martinez et al., 2000), with the main assumptions being that the system is in steady-state balance between sources and losses of NO_3 and N_2O_5, $d[NO_3]/dt = d[N_2O_5]/dt = 0$, and that equilibrium in the NO_2-NO_3-N_2O_5 system has been established. If such is the case, then the steady-state lifetime of NO_3 is defined by:

$$\tau_S(NO_3) = \frac{[NO_3]}{k_1[O_3][NO_2]} \quad (3)$$

A recent report (Brown et al., 2003a) discusses in detail the difference between the assumptions of steady-state and equilibrium, and illustrates convincingly that although equilibrium can be achieved very rapidly, the approach to steady-state can take much longer, on the order of several hours,

especially under conditions of high NO_2 and low temperatures. Lifetimes calculated using the steady-state approximation can be significantly biased in such cases, and the conclusions made from analysis of the lifetimes are cast in doubt. Considering the high levels of NO_2 encountered in this study, we found it prudent to calculate lifetimes of NO_3 without invoking the steady-state assumption using a relatively easy approach, but not reported previously to the best of our knowledge. We assume that the equilibrium shown in Eq. (1) is valid, and use our previous argument of fast turnover times at warm temperatures encountered in the study as evidence that equilibrium is, in fact, achieved rapidly. To derive an expression for the non steady-state lifetimes of NO_3, we formally consider a combined reservoir of NO_3 and N_2O_5, ($[NO_3]$+$[N_2O_5]$), that has both sources and losses. Chemical interchanges between NO_3 and N_2O_5 (Reactions R2f, R2r) do not need to be considered, since a gain or loss of a molecule of NO_3 also results in a gain or loss of a molecule of N_2O_5, for a null change in the reservoir. The continuity equation for the reservoir, ignoring fluxes, is:

$$\frac{\mathrm{d}\{[NO_3]+[N_2O_5]\}}{\mathrm{d}t} = S_{NO_3+N_2O_5} - L_{NO_3+N_2O_5} \quad (4)$$

The only known significant source to the reservoir is the production of NO_3 via Reaction (1):

$$S_{NO_3+N_2O_5} = k_1[O_3][NO_2] \quad (5)$$

The losses from the reservoir will occur through external losses of NO_3 or N_2O_5 that can be parameterized as pseudo first order losses:

$$L_{NO_3+N_2O_5} = L_{NO_3} + L_{N_2O_5} = k_x[NO_3] + k_y[N_2O_5] \quad (6)$$

where k_x and k_y are the overall pseudo first order rate constants for NO_3 and N_2O_5 respectively. Combining Eqs. (4), (5) and (6) we obtain:

$$k_1[O_3][NO_2] - \frac{\mathrm{d}[NO_3]}{\mathrm{d}t} - \frac{\mathrm{d}[N_2O_5]}{\mathrm{d}t} = k_x[NO_3] + k_y[N_2O_5] \quad (7)$$

The lifetime of NO_3 can generally be defined as the ratio of the concentration of NO_3 to the losses of NO_3, L_{NO_3}:

$$\tau_{NO_3} = \frac{[NO_3]}{L_{NO_3}} \quad (8)$$

For the combined reservoir, we can define the lifetime of NO_3, $\tau^*_{NO_3}$, including direct and indirect losses from the reservoir:

$$\tau^*_{NO_3} = \frac{[NO_3]}{L_{NO_3+N_2O_5}} \quad (9)$$

Substituting Eqs. (4) and (5) into Eq. (9) we get:

$$\tau^*_{NO_3} = \frac{[NO_3]}{k_1[O_3][NO_2] - \frac{\mathrm{d}[NO_3]}{\mathrm{d}t} - \frac{\mathrm{d}[N_2O_5]}{\mathrm{d}t}} \quad (10)$$

Note that $\tau^*_{NO_3} = \tau_S$ (NO_3) if $\mathrm{d}[NO_3]/\mathrm{d}t = \mathrm{d}[N_2O_5]/\mathrm{d}t = 0$. Equation (10) represents a way to calculate the apparent lifetime of NO_3 in the NO_2-NO_3-N_2O_5 equilibrium system without assuming steady-state, if one has continuous measurement data for NO_3, O_3, NO_2, and N_2O_5. It is possible to find the derivatives, $\mathrm{d}[NO_3]/\mathrm{d}t$ and $\mathrm{d}[N_2O_5]/\mathrm{d}t$ by calculating the rate of change of NO_3 and N_2O_5 with respect to time from the observational data. If measurements of $[N_2O_5]$ are not available, $[N_2O_5]$ can be calculated from Eq. (1) if it can be shown that equilibrium is established. We have used this latter approach in the current study. The derivatives, $\mathrm{d}[NO_3]/\mathrm{d}t$ and $\mathrm{d}[N_2O_5]/\mathrm{d}t$, were calculated using a three point running slope in the continuous data set. This approach introduces more noise into the calculation of the NO_3 lifetime, but has the benefit of unbiased lifetimes. The approach assumes that $\mathrm{d}[NO_3]/\mathrm{d}t$ and $\mathrm{d}[N_2O_5]/\mathrm{d}t$ are the rates of change due to chemistry alone. The lifetimes will be biased if the changes are due to rapid transport effects, as would also generally be true for steady-state lifetime calculations. In our analysis, we assume that the air surrounding the site is sufficiently homogeneous such that rapid transport effects can be neglected, although there will likely be some times when this is not true, which are difficult to determine without auxiliary data. Other lifetimes can be calculated for the reservoir depending on preference and application. One can define the lifetime of N_2O_5, $\tau^*_{N_2O_5}$, including direct and indirect losses of N_2O_5 from the reservoir:

$$\tau^*_{N_2O_5} = \frac{[N_2O_5]}{L_{NO_3+N_2O_5}} \quad (11)$$

In this paper, we focus on the non steady-state lifetime of NO_3, $\tau^*_{NO_3}$, as it allows comparison to previous studies and also allows us to separate the losses of NO_3 and N_2O_5 from the equilibrium system as shown below. Dividing Eq. (7) by $[NO_3]$ we obtain

$$\frac{k_1[O_3][NO_2] - \frac{\mathrm{d}[NO_3]}{\mathrm{d}t} - \frac{\mathrm{d}[N_2O_5]}{\mathrm{d}t}}{[NO_3]} = k_x + k_y\frac{[N_2O_5]}{[NO_3]} \quad (12)$$

or expressed slightly differently, we write

$$(\tau^*_{NO_3})^{-1} = k_x + k_y\frac{[N_2O_5]}{[NO_3]} = k_x + k_yK_{eq}[NO_2] \quad (13)$$

This is the same equation presented previously by others (Allan et al., 2000; Brown et al., 2003a), with the exception that we use inverse *non* steady-state lifetimes instead of inverse steady-state lifetimes. This expression allows the determination of the overall first order rate constants for loss of NO_3 and N_2O_5, k_x and k_y, from the intercept and slope of a plot of $(\tau^*_{NO3})^{-1}$ versus $K_{eq}[NO_2]$, or equivalently, $(\tau^*_{NO_3})^{-1}$ versus $[N_2O_5]/[NO_3]$.

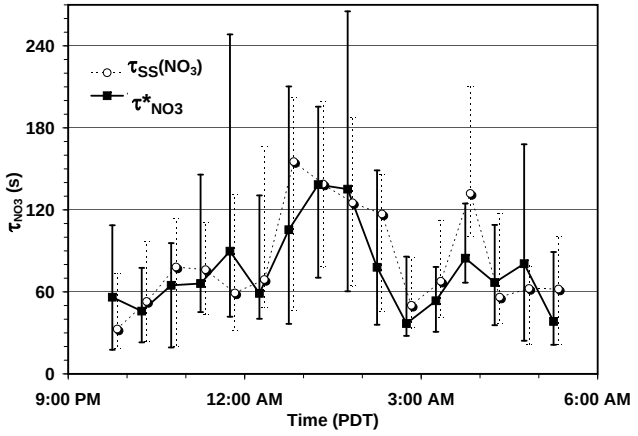

Fig. 7. Study wide nocturnal variation in median NO_3 lifetimes, including the non steady-state (non-SS) lifetimes calculated using Eq. (10), and the steady-state (SS) lifetime calculated using Eq. (3), offset by +5 min for clarity. Error bars indicate the 25th and 75th percentiles of the distributions.

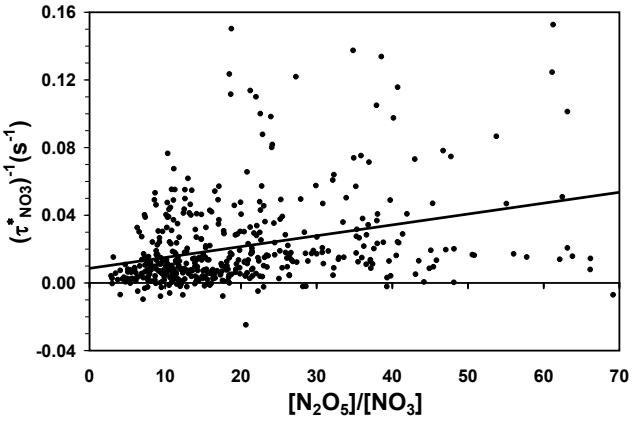

Fig. 8. Variation of inverse lifetime of NO_3 with N_2O_5/NO_3 ratio, including all 8 p.m.–8 a.m. data. Least squares analysis gives: intercept= $k_x = 0.0087 \pm 0.0020\,\mathrm{sec}^{-1}$; slope= $k_y = 5.72(\pm 0.81) \times 10^{-4}\,\mathrm{s}^{-1}$, as seen in Eq. (13).

4.3.2 Observations of NO_3 lifetime and losses

The observed distribution of NO_3 lifetimes throughout the study calculated according to Eq. (10) and via Eq. (3) are given in Table 1. The median values are similar, between 1–1.5 min, although there are differences at the extremes of the distribution between steady-state and non steady-state predictions. The temporal variation of lifetimes calculated using the two methods are shown in Fig. 7. Surprisingly, the nocturnal patterns look similar although there are subtle differences. During periods when the nocturnal pool of NO_3 and N_2O_5 is building such as early evening, $d[NO_3]/dt$ and $d[N_2O_5]/dt$ are positive, and we would expect the steady-state assumption to predict lifetimes that are shorter than the true lifetime. This is true on average before midnight using the data seen in Fig. 7, although only marginally so. The reverse would be true during periods when the nighttime reservoir pool is depleting rapidly; $d[N_2O_5]/dt$ and $d[NO_3]/dt$ are negative and the steady-state lifetime is expected to be larger than the true lifetime. This trend is somewhat more obvious in Fig. 7, perhaps due to the lower temperatures during the latter part of the night that slows the kinetics and the approach to steady-state. It is likely that overall, the relatively warm nighttime temperatures encountered in this study (Table 1) assist in a more rapid approach to steady-state than that encountered in the previous modeling study by Brown (2003; 12 °C), where the differences between $\tau_S(NO_3)$ and $(k_{NO_3})^{-1}$ were more obvious. For example, the thermal decomposition of N_2O_5 (Reaction R2r), has a rate of reaction that more than doubles by increasing the temperature from 12 °C to 18 °C. It is also true that the shorter lifetimes encountered in this study compared to those in Brown (ie-greater reactivity of NO_3 and N_2O_5) lead to better agreement between the steady state and non steady state assumption. The median and average NO_3 lifetimes of 1–1.5 min and 2–2.5 min calculated here can be compared to other studies in the MBL; ∼4.2 min annual average in the Baltic sea (Heintz et al., 1996), ∼3 min in the summer Mediterranean (Vrekoussis et al., 2004), between 1 and 20 min in the north east and central east Atlantic (Allan et al., 2000), and between 0.2 to 17 min in a coastal region off Germany (Martinez et al., 2000). A general observation in the above studies is that the lowest lifetimes are observed under the influence of polluted air masses. Our results are consistent with this.

Regression of $(\tau^*_{NO_3})^{-1}$ with $[N_2O_5]/[NO_2]$ for all nighttime data is shown in Fig. 8. The r^2 for the regression is only 0.10, implying that only 10% of the variance can be accounted for by the correlation with $[N_2O_5]/[NO_3]$. Nonetheless, as suggested by Eq. (13), the intercept and slope provide overall first order rate constants for loss of NO_3 and N_2O_5 respectively: $k_x = 0.0087 \pm 0.0020\,\mathrm{s}^{-1}$, $k_y = 5.72(\pm 0.81) \times 10^{-4}\,\mathrm{s}^{-1}$. These can at best be interpreted as average rate constants encountered for the entire study, as undoubtedly, the rate constants would vary depending on many parameters including the air mass origin, air mass history, time of night, temperature and other meteorological conditions. Interpreting the values of k_x and k_y as study average constants, the relative losses of NO_3 via direct versus indirect losses can easily be determined by comparing the magnitude of k_x with $k_y[N_2O_5]/[NO_3]$. Using a study central ratio of $[N_2O_5]/[NO_3] = 15$ (median=13.1, average=16.8), we determine that 50.4±13.2% of losses of NO_3 are direct, compared to 49.6±9.6% of losses that are indirect through losses of N_2O_5. This result is consistent with recent estimates of direct and indirect losses of NO_3 in a study on Appledore Island 10 km off the coast of Maine (Ambrose et al., 2007).

One approach to remove much of the variability in the previous methodology is to analyze subsets of the data according to time bins. The rationale is that many parameters follow general trend patterns during the night; temperature decreases, relative humidity increases, wind speeds decrease, reactive VOCs decrease, to name a few. Figure 9 shows the results of such an analysis in which hourly binned data from the study are regressed according to Eq. (13) to determine the nocturnal pattern in k_x and k_y. As can be seen, a dramatic decrease in the value of k_x occurs in the first few hours of the night, to values that are zero within statistical error. This apparent decay of k_x would be consistent with oxidation and significant depletion of species that have significant reactivity with NO_3, many of which may have significant daytime fluxes. Ignoring photolysis and the assumed slow heterogeneous loss of NO_3, the value of k_x at night would be given by the following equation:

$$k_x = k_4[NO] + \sum_i k_{7i,NO_3}[VOC]_i \quad (14)$$

where k_4 is the rate constant for Reaction (R4) and k_{7i,NO_3} is the rate constant for Reaction (R7), that of NO_3 with an individual VOC_i. As no ancillary measurements of NO or VOCs were made at the location, we cannot confirm the magnitude of the direct sink of NO_3 from these reactions, although it is known that the region is influenced by NO_x emissions from ship plumes (Lu et al., 2006), large fluxes of DMS (Sharma et al., 2003), α-pinene (McLaren et al., 2004), isoprene and a range of anthropogenic VOCs (Jiang et al., 1997). Temporal profiles in the MBL in other regions indicate that rapid depletion of DMS due to reaction with NO_3 occurs during the first few hours after sunset (Vrekoussis et al., 2004). Depletions of monoterpenes and isoprene by NO_3 after sunset are also known to occur in continental areas (Geyer et al., 2001; Brown et al., 2009), as are certain reactive anthropogenic hydrocarbons (Dimitroulopoulou and Marsh, 1997). Using rate constants for the reaction of NO_3 with VOCs (Atkinson et al., 2004; Atkinson et al., 2006), the value of k_x observed early in the evening (k_x =0.034 s^{-1}) would be consistent with individual reactions of NO_3 with 52 ppt of NO, 1.2 ppb DMS, 1.9 ppb isoprene, 219 ppt α-pinene, 4.0 ppb i-butene, ~100 ppt of any isomer of cresol, or an appropriate mixture of the above. The summer time flux of DMS from the Strait of Georgia has recently been estimated to be 2.2 µmol m^{-2} day^{-1} (Sharma et al., 2003). Using this flux and assumptions of a boundary marine layer height of 100 m, [OH]= 2.5×10^6 molec cm^{-3} during day, [NO_3] = 2.5×10^8 molec cm^{-3} (10 ppt) at night, $k_{OH,DMS}$ = 6.5×10^{-12} $molec^{-1}$ cm^3 s^{-1} and $k_{NO_3,DMS}$ = 1.1×10^{-12} $molec^{-1}$ cm^3 s^{-1} (Atkinson et al., 2004), a simple box model analysis predicts a daytime concentration of DMS that builds to 200 ppt at sunset, followed by a rapid decline over a few hours to a steady-state value of 22 ppt in the latter parts of the night. Combining this information with the early evening value of k_x leads us to conclude that DMS is not the main sink for NO_3 in the early evening, although NO_3 is likely the main sink for DMS. Further study with ancillary measurements of VOCs would be needed to confirm the magnitude of the direct sink for NO_3 reported here, and to determine the relative contribution of each hydrocarbon.

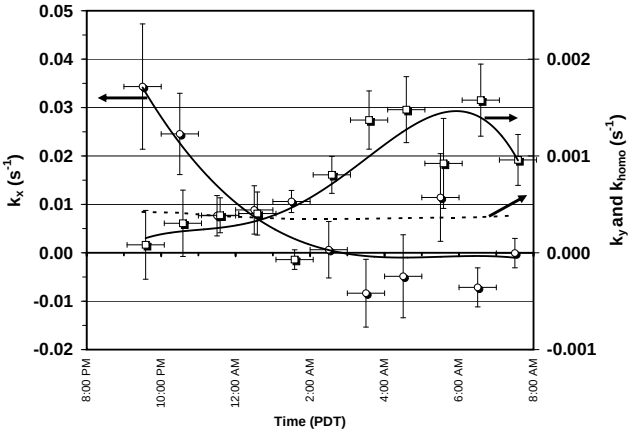

Fig. 9. Nocturnal variation of overall first order rate constants for loss of NO_3, k_x (open circles) and N_2O_5, k_y (open squares), predicted by fitting hourly binned data to Eq. (13). The dashed line represents k_{homo}, the pseudo first order rate constant for the homogeneous reaction of N_2O_5 with H_2O vapor (see text). Solid lines are 4th order polynomials meant to show the general trend only. Error bars show the standard error of the fit coefficients.

The value of k_y observed in Fig. 9 is roughly constant for the first few hours of the night and then increases in the latter parts of the night. Losses of N_2O_5 are thought to occur through homogeneous reactions with H_2O (Reaction R10), with the current uncertain recommendation (Atkinson, 2004) of both a first order and second order dependence on H_2O based upon recent work (Wahner et al., 1998), and through heterogeneous reactions on the surface of aerosols to produce HNO_3 (Reaction R9), $ClNO_2$ (Reaction R11) and Cl_2 (Reaction R12b). The overall pseudo first order rate constant for loss of N_2O_5, k_y, could be expressed as:

$$k_y = k_{homo} + k_{het} = k_{10a}[H_2O] + k_{10b}[H_2O]^2 + \frac{\gamma A}{4}\sqrt{\frac{8RT}{\pi M}} \quad (15)$$

where $k_{10a} = 2.5\times10^{-22}$ cm^3 $molecule^{-1}$ s^{-1}, $k_{10b} = 1.8\times10^{-39}$ cm^6 $molecule^{-2}$ s^{-1}, γ is the uptake coefficient of N_2O_5 on the aerosol, A is the surface area of the aerosol, R is the gas constant and M is the molecular mass of N_2O_5. Based upon measured water concentrations at the site, the magnitude of k_{homo}, given by the first two terms in Eq. (15), was calculated for all observations and has been plotted in Fig. 9 as the dotted line. The last term in Eq. (15) is equivalent to the rate constant for heterogeneous reactions of N_2O_5 on aerosols, k_{het}, a simplification of the Fuchs and Sutugin equation (Fuchs and Sutugin, 1971) for γ <0.1. Without ancillary measurements of aerosol surface area, we are not

able to determine the magnitude of the last term in (Reaction R15), although we can estimate it by difference.

It is noted that the magnitude of the observed value of k_y during the first few hours after sunset is consistent with the homogeneous gas phase hydrolysis rate of N_2O_5, k_{homo}. Despite this, our result cannot be used as proof that the homogeneous reaction is indeed occurring at this rate since we do not know k_{het}. Recent field studies have been inconclusive on this point, with one study showing some agreement between observed homogeneous loss rates and the recommended hydrolysis rate (Ambrose et al., 2007) while others have found the recommended homogeneous hydrolysis rate coefficient to be too large (Brown et al., 2009).

The value of k_y increases after 2 a.m. to values that are statistically greater than k_{homo}, indicating that heterogeneous reactions of N_2O_5 on aerosols become more significant at this time. The average relative humidity at Saturna increased from ~68% just after sunset to a maximum of 82% just before sunrise. The timing of the increase in k_y at 1–2 a.m. roughly corresponds to the time when the relative humidity increases beyond the deliquescence relative humidity (DRH) point for sea salt aerosols, 70–75% (Tang et al., 1997). This may indicate that the marine air mass contains dry sea salt aerosols or possibly other types of dry aerosols early in the night. It seems unlikely that the MBL contains locally generated dry sea salt aerosols as the relative humidity was always >50% at night, which is greater than the efflorescence relative humidity (ERH) of sea salt, 43–48% (Tang et al., 1997), the RH we would expect is needed for production of dry sea salt aerosols. It is possible that the MBL contains dry sea salt aerosols through other mechanisms such as mixing of marine air with dry air through subsidence, or for the marine air mass to have part of its back trajectory over drier terrestrial regions. The latter could be accomplished through classic sea/land breeze recirculation during the day/night that is well characterized in this region (Hedley and Singleton, 1997). In another study (Vrekoussis et al., 2007), it was observed that the correlation between $\ln(\tau_{NO_3})$ and $\ln(NO_2)$, became more negative as RH increased, taken as evidence that supports the existence of indirect sinks of NO_3 that are related to the presence of water vapor in the atmosphere. We note that while RH increases through the night, the absolute concentration of water is roughly constant, or actually decreases slightly as the night progresses. As such, the results presented here strongly suggest that the increased indirect sinks of NO_3 with increasing relative humidity are not related to the homogeneous loss of N_2O_5, but are related to the heterogeneous loss of N_2O_5. However, we also observe that the losses of N_2O_5 via the homogeneous hydrolysis mechanism may not be insignificant, ranging in this study from up to 100% early in the night to a minimum of up to 23% later in the night, although this should be tempered by the uncertain nature of the current recommendation for the homogeneous rate constant of N_2O_5 with H_2O.

The values of k_y observed here, ranging from zero (within error), to $\sim 1.6\times10^{-3}\,s^{-1}$, are within the range of values of $(\tau_{N_2O_5})^{-1}$ reported in other studies of calculated N_2O_5 in the MBL (Heintz et al., 1996; Martinez et al., 2000). Subtracting k_{homo} from k_y (see Eq. 15), we obtain an estimate of k_{het}, which ranges from zero (within error) in the first part of the night to a maximum of $1.2\times10^{-3}\,s^{-1}$ in the latter part of the night. In the polluted subtropical MBL, Osthoff et al. (2008) modeled their observations of NO_x, NO_3, N_2O_5, $ClNO_2$ and O_3 in order to estimate the magnitude of the overall loss of N_2O_5, included a heterogeneous reaction of N_2O_5 that produces just HNO_3, and another heterogeneous reaction that produces HNO_3 and $ClNO_2$. The observed values of the combined loss coefficient of N_2O_5 for two case studies they presented were $3\times10^{-3}\,s^{-1}$ and $1.0\times10^{-3}\,s^{-1}$. The maximum values of k_y observed in Fig. 9 are within the range simulated by Osthoff et al. (2008).

4.4 Relationship between nighttime chemistry and O_3 formation in the Lower Fraser Valley

To look for a link between nighttime chemistry in the MBL of the Strait of Georgia and ozone formation in the LFV, we performed a semi-observational analysis using observational data of ozone at multiple monitoring stations in the valley and correlating these with overnight integrated concentrations of N_2O_5 at Saturna. A brief description of the rationale and approach follows.

The potential products in the heterogeneous and homogeneous reactions of N_2O_5 are HNO_3, $ClNO_2$, Cl_2, and potentially others.

$$N_2O_5 \xrightarrow{\text{sea salt aerosols}} HNO_3, ClNO_2, Cl_2, \text{ others} \qquad (16)$$

The rate of production of a product p_i, from one of these reactions is given by:

$$\frac{dp_i}{dt} = k_{het,i}[N_2O_5] \qquad (17)$$

The value of the individual pseudo first order rate constants, $k_{het,i}$ are uncertain and are current source of research interest at this time. For photolabile species such as $ClNO_2$, and Cl_2 that have few losses at night, accumulation will occur overnight such that the total accumulated concentration by morning, $P_i(t)$, assuming constant conditions, is given by:

$$P_i(t) = \int_0^t k_{het,i}[N_2O_5]dt = k_{het,i}\int_0^t [N_2O_5]dt \qquad (18)$$

Production stops in the morning due to the short lifetime of NO_3 and N_2O_5 during sunlit hours. It can be seen that the accumulated concentration is proportional to the integral of the N_2O_5 concentration with respect to time overnight, and proportional to the heterogeneous rate constant that describes

the rate of formation of p_i from N_2O_5. Here we will make the assumption that the overnight integrated concentration of N_2O_5 at East Point is representative of the general conditions that occur in the MBL of the Strait overnight, and that the overnight integral of N_2O_5 can be used as a surrogate for the amount of accumulated photolabile species each morning, without knowledge of the individual heterogeneous rate constants, $k_{het,i}$. The overnight integral was calculated for each night using a summation over the N observations between 8 p.m. and 8 a.m.:

$$\int_0^t [N_2O_5]dt = \sum_{j=1}^{N} [N_2O_5]_j \times (t_{end,j} - t_{start,j}) \quad (19)$$

where $t_{end,j}$ and $t_{start,j}$ are the end and start times of the jth observation. The overnight N_2O_5 integral at East Point ranged from 6.7×10^{13} to 4.9×10^{14} molecules cm^{-3} sec, or 0.061–0.444 ppb-nights, where the unit "night" is defined in this context as a 12.0 h overnight period.

Before going further, it is interesting to estimate how much $ClNO_2$ could be produced on such nights in the presence of sea salt aerosol. Using a lower end heterogeneous rate constant for the production of $ClNO_2$ from a recent study (Osthoff et al., 2008), $k_{het,ClNO_2} = 1.0\times10^{-4}\,s^{-1}$, we calculate potential $ClNO_2$ accumulations ranging from 0.26–1.9 ppb over the course of thirteen nights, with a median amount of 0.73 ppb. The question of Cl^- availability in the marine aerosol to produce such levels of $ClNO_2$ arises. To answer this question, we have analysed data from a previous study (Anlauf et al., 2006) in the LFV where size segregated aerosol ionic composition was measured at several stations over the course of several weeks. Using 90th to 100th percentiles of the total Na^+ composition in aerosols measured at Langley and Slocan (close to T27 and T4, Fig. 1) as representing diluted marine air, and applying a Cl/Na molar ratio of 1.17 in sea water (Seinfeld and Pandis, 2006), we estimate that the Cl^- content of the marine aerosol in the Strait contains minimum levels of 0.8–1.3 ppbV chloride, expressed as a gas mixing ratio for suitable comparison. Measured accumulations higher than this would need to invoke other mechanisms of $ClNO_2$ formation such as uptake of HCl on Cl^- deficient sea salt aerosols (Osthoff et al., 2008), or the more recent report of heterogeneous reactions of N_2O_5 and HCl on surfaces (Raff et al., 2009).

Another approach we could use to estimate the overnight accumulation of $ClNO_2$ is taken from the modeling study by Simon et al. (2009). They used the observation from Osthoff et al. (2008) that 11–61% of the source of the nighttime NO_3/N_2O_5 reservoir, namely Reaction (R1), is converted to $ClNO_2$. They used the lower estimate of 10% and a modified reaction as a source of $ClNO_2$ in their model, $NO_2{+}O_3 \rightarrow 0.9\ NO_3 + 0.1ClNO_2{+}O_2$. In a similar way, and using a lower limit conversion of 11% from Osthoff et al. (2008), we calculated $ClNO_2$ accumulations from the integral,

$$ClNO_2(t) = 0.11 \int_0^t k_1[NO_2][O_3]dt \quad (20)$$

Using this second approach, we calculated overnight $ClNO_2$ accumulations ranging from 0.31–1.6 ppb, with a median amount of 0.77 ppb, similar to the estimate by the first method. Nevertheless, the first method is more desirable since it is directly linked to the reactant N_2O_5, and would not suffer from cases of strong direct losses of NO_3 in the marine boundary layer that do not lead to production of $ClNO_2$. Both methods for estimating $ClNO_2$ accumulations suffer from very uncertain observational parameters, either the heterogeneous rate constant to produce $ClNO_2$ or the overall conversion efficiency, in addition to being unconstrained by actual observations of photolabile halogen species. In the methodology to follow, we examine links to ozone formation using overnight integrals of N_2O_5.

The effect, if any, of overnight accumulated photolabile species will be experienced in the LFV the next day only if there is transport of marine air from the Strait into the valley. Meteorological observational data from 6 stations (see location in Fig. 1) in the valley were examined to look for evidence of a sea breeze each day. A sea breeze in this region has been identified similar to that of others (Snyder and Strawbridge, 2004), through examination of the wind direction (WD) vectors:

$$\text{Inflow (sea breeze)} \equiv 180^\circ < WD < 330^\circ \quad (21)$$

$$\text{Outflow (land breeze)} \equiv 0^\circ < WD < 120^\circ \quad (22)$$

To assess transport of marine air from the Strait into the LFV, a simple criterion was applied that required evidence of sustained inflow for several hours, with wind speeds >5 km h^{-1}, at all 6 stations the following day. Considering 13 nights when overnight integrals of N_2O_5 were available, sea breezes were observed on 9 of the days that followed, with 4 of the days showing either no evidence or only partial evidence of a sea breeze. The 9 nights retained for subsequent analysis included 24/25, 25/26, 26/27, 27/28, 31 July/1, 1/2, 3/4, 5/6 and 6/7 August. The average wind vectors for afternoon hours on the 9 days when the sea breeze was well developed (12–4 p.m.) were: Vancouver International (WD = 286°, WS = 17.6 km h^{-1}), Sandheads (WD = 287°, WS = 17.3 km h^{-1}), Pitt Meadows (WD = 258°, WS = 7.8 km h^{-1}), White Rock (WD = 228°, WS = 6.8 km h^{-1}), Abbotsford (WD = 229°, WS = 11.6 km h^{-1}) and Hope (WD = 290°, WS = 19.9 km h^{-1}). A general observation of the meteorological analysis is that sea breezes start and finish earlier for those stations close to the coast, compared

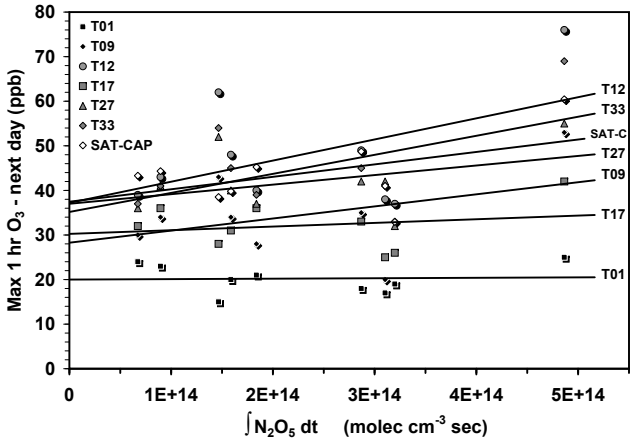

Fig. 10. Correlation of integrated N_2O_5 concentration with respect to time over the course of the night and maximum 1 h average ozone the next day seen at monitoring stations in the Lower Fraser Valley. The analysis includes only nights in which a significant observable sea breeze was observed the next day have been included.

to those stations further inland (i.e. – Abbotsford and Hope). It should also be mentioned that there is evidence from previous studies in this area that sea salt aerosols are carried by the sea breeze very far inland, further than Abbotsford. These aerosols show classic Cl^- deficiency compared to Na^+ due to heterogeneous reaction with N_2O_5 at night and/or HNO_3 displacement reactions during the day (McLaren et al., 2004; Anlauf et al., 2006).

In the semi-observational approach, regression analysis was performed separately for each monitoring station in the domain. Regression analysis was performed between the maximum 1-h average O_3 values at a station on the day following each overnight period and the corresponding overnight N_2O_5 integrals, our surrogate for nighttime chemistry and accumulated amount of photolabile species. An example of the regressions for a few representative stations is given in Fig. 10. Linear regression analysis was used to determine the slope of the relationship, $dO_3/d\int[N_2O_5]dt$. A zero slope indicates no effect (null hypothesis) while a positive slope of statistical significance indicates that there is a correlation between the overnight N_2O_5 integral at East Point and ozone formation at the station the following day. We refer to the next day as Day+0.5 since it follows ∼12 h after the nighttime period. Most of the stations shown in Fig. 10 indicate a positive correlation between O_3 and integrated N_2O_5, although only one station (T33) has a slope that is statistically different from zero at the 90 percent confidence level. The correlations are weak in general, with r^2 ranging from close to zero for stations that have negligible slopes (e.g. T01: $r^2 = 0.0015$), to $r^2 = 0.28$ for station T33 in Abbotsford. At Abbotsford, this indicates that while the correlation is statistically significant, only 28% of the variance in peak ozone levels can be linked to a relationship with nighttime chemistry in the marine boundary layer. This might be expected as there are many other important variables that contribute to ozone formation. The number of stations showing a positive correlation though, can add confidence that there is a real effect; 18 of the 20 stations show a positive correlation (Table 2). An average correlation for all the stations in the LFV gives more statistical confidence, indicating that the average value of the correlation, $dO_3/d\int[N2O5]dt$ is $(1.72\pm0.43)\times10^{-14}$ ppb O_3 cm^3 molec^{-1} s^{-1}, is statistically significant at the 95% confidence level. This can be converted to a slightly more palatable set of units, $dO_3/d\int[N_2O_5]dt = 18.8\pm4.8$ ppb $O_3\times$ppb $N_2O_5^{-1}$ night^{-1}. We can estimate the range of the average ozone increase, ΔO_3, that would be associated with the overnight accumulation by multiplying the slope by the range of $\int[N_2O_5]dt$ observed in the study, expressed previously (0.061–0.444 ppb N_2O_5·nights). This gives us a range of $\Delta O_3 = +1.1$ to $+8.3$ ppb O_3 (peak average hourly) for an average station in the LFV. We expect values outside this range for individual stations as there will be variation in the effect dependent on the location of the station. The positive relationship between overnight integrated N_2O_5 and maximum O_3 the next day when there is a definitive transport of marine air into the LFV can be explained in many ways. As suggested previously, the photolabile products of the heterogeneous reaction of N_2O_5 on sea salt aerosols, such as $ClNO_2$ and Cl_2, can photolyze upon sunset to produce Cl atoms (Reaction R14). The Cl atoms, being very reactive, will react with reactive hydrocarbons to produce alkyl radicals, R. and HCl (Reaction R15). Following this, the reaction sequence will lead to ozone formation following the well known photochemical O_3 formation mechanism, including generation of peroxy radicals (Reactions R16), oxidation of NO to NO_2 and production of alkoxy radicals (Reactions R17), photolysis of NO_2 to produce oxygen atoms (Reactions R18), which then combine with molecular oxygen to form O_3 (Reactions R19).

$$Cl^{\cdot} + RH \rightarrow HCl(g) + R^{\cdot} \quad \text{(R15)}$$

$$R^{\cdot} + O_2 \rightarrow RO_2^{\cdot} \quad \text{(R16)}$$

$$RO_2^{\cdot} + NO \rightarrow RO^{\cdot} + NO_2 \quad \text{(R17)}$$

$$NO_2 + h\nu \rightarrow O(^3P) + NO \quad \text{(R18)}$$

$$O(^3P) + O_2 + M \rightarrow O_3 + M \quad \text{(R19)}$$

Several recent modeling studies have tried to estimate the amount of ozone that would be generated by a realistic influx of Cl atoms into coastal domains, either from $ClNO_2$ or Cl_2, and more recently from ClNO. The range of ozone effects that have been published, ΔO_3, range from $+1.0$ ppb to $+9$ ppb for $ClNO_2$ in Houston (Osthoff et al., 2008; Simon et al., 2009), $+4$ to $+12$ ppb for Cl_2 in the California South Coast Air Basin (Knipping and Dabdub, 2003), and up to $+40$ ppb for ClNO in regions downwind of Los Angeles

Table 2. Correlation between $\int N_2O_5 dt$ measured overnight at Saturna Island and maximum 1-h ozone measured at air monitoring stations in the LFV the next day (DAY +0.5) and the day after that (Day +1.5).

	Day+0.5		Day+1.5	
Station	$dO_3/d\int N_2O_5 dt$ ppb O_3ppb $N_2O_5^{-1}$ night^{-1}	r^2	$dO_3/\int N_2O_5 dt$ ppb O_3ppb $N_2O_5^{-1}$ night^{-1}	r^2
T01	+1.1±10	0.002	+29.1±9.9	0.551
T02	+15.2±15	0.131	+3.0±9.9	0.013
T04	+19.9±16	0.178	−1.5±7.9	0.005
T06	+0.3±13	0.000	+17.5±8.6	0.375
T09	+29.7±26	0.153	+9.3±14	0.057
T12	+51.9±35	0.235	+27.5±23	0.164
T13	+0.4±18	0.000	−2.0±14	0.003
T14	+30.3±18	0.280	+21.8±11	0.352
T15	+9.0±18	0.033	+25.8±17	0.257
T17	+9.0±16	0.041	+26.6±13	0.388
T18	−2.2±9	0.009	+2.6±8.2	0.014
T20	+12.3±18	0.059	+28.5±14	0.368
T26	+2.3±13	0.004	+23.2±17	0.213
T27	+23.6±21	0.153	+13.6±19	0.066
T29	+30.6±37	0.088	+33.1±34	0.116
T30	+31.0±23	0.201	+37.8±18	0.369
T31	−2.3±14	0.004	+32.4±18	0.311
T32	+36.8±27	0.209	+11.3±14	0.085
T33	+46.8±28	0.281	+19.6±19	0.130
CAPMon	+30.6±21	0.236	+9.5±26	0.019

(Raff et al., 2009). It is understood that there are vast differences in the models, modelling approaches, and assumptions about the emission rates of the photolabile species in these models.

To further test the null hypothesis, the regression analysis was extended to include the maximum hourly O_3 formed at each station for the two days previous, and the two days following the next day after the nighttime accumulation. We describe these as Days −1.5, −0.5, +0.5, +1.5 and +2.5 with the central day, Day +0.5, referring to the daytime period immediately following a nighttime accumulation. In a similar way as described for the initial Day +0.5 case, the average response for all stations was calculated. The average response for all the stations as a function of day is presented in Fig. 11, with error bars indicating the standard error (1σ). The results for the station by station regressions are shown for Day +0.5 and Day +1.5 in Table 2. The results presented in Fig. 11 indicate that there is a positive effect on Day 0.5 as previously discussed, and an almost equivalent effect on Day 1.5, with the effect disappearing by Day 2.5. As we will see shortly, the residual effect on Day 1.5 is spatially different than that seen on Day 0.5. Furthermore, while the average effect at the stations is the same or marginally less on Day 1.5 compared to Day 0.5, many of the correlations on Day 1.5 (see Table 2) are much higher than Day 0.5, with 7 stations showing a statistically significant effect at 90% confidence,

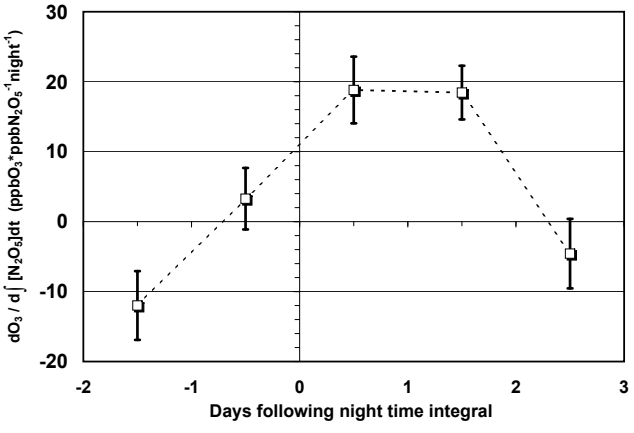

Fig. 11. Average response of peak hourly average ozone at monitoring stations in the valley to overnight integral of N_2O_5 with respect to time in the marine air of the Strait, for days following a nighttime integral. Day +0.5 corresponds to the day immediately following a nighttime measurement. The analysis includes only nights in which a significant observable sea breeze was observed the next day.

5 stations at the 95% confidence level. The lack of an effect on days before the nighttime accumulation (Days −0.5 and −1.5) rules out the possibility that the accumulation of N_2O_5 is caused by high O_3 events in the days preceding the event.

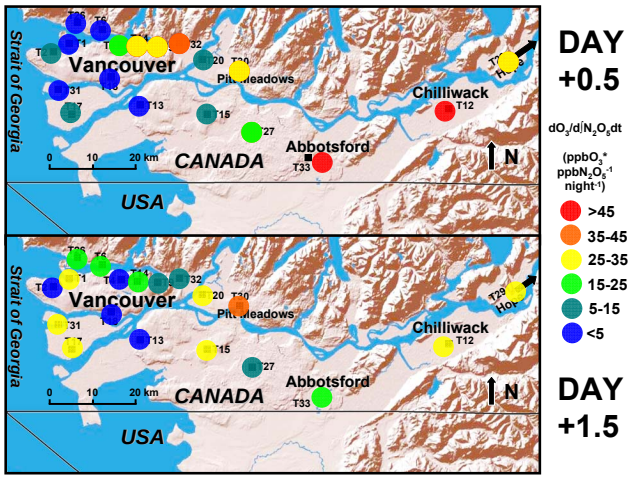

Fig. 12. Spatial variation in response of peak hourly average ozone at monitoring stations in the valley to overnight integral of N_2O_5 with respect to time in the marine air at Saturna Is., for days following a nighttime integral. Day +0.5 (top panel) and Day +1.5 (bottom panel) correspond to the day immediately following a nighttime integral, and the day after that respectively.

This also adds confidence that the higher ozone in the LFV is caused by nighttime chemistry in the Strait, and is not just casually correlated with it.

There are many possible explanations for a residual effect on Day 1.5. A comparison of the spatial variability of $dO_3/d\int[N_2O_5]dt$ on Day +0.5 and Day +1.5, Fig. 12, will enlighten this discussion. On Day 0.5, there is a general trend of low correlation for stations close to the coast, especially around the urban area of Vancouver, and larger correlation downwind in the valley. The largest effect is seen between Abbotsford and Chilliwack. Using wind vectors established previously, we estimate average transport times from the coast to Abbotsford and Chilliwack of 5–8 h and 8–10 h respectively during days with sea breezes. The larger effect seen at these stations is likely the result of chemical amplification that occurs with longer reaction times. Although reactive photolabile species would long be depleted by the time air is transported to these sites, the effect of a morning burst of radicals coincident with a morning sea breeze developing close to the coast will contribute more significantly to ozone formation as time proceeds. The small effect seen at coastal stations is likely the result of the shorter transport time from the coast. It is also noted that on Day 0.5, there is a cluster of increased effect along the north side of Vancouver (stations T4, T9, T14, and T32). This is an area concentrated in with industrial activity including refineries. It is suspected that increased VOC emissions in this area could be responsible for the increased effect.

The spatial variability of the correlation on Day 1.5 is very much different than the previous day. Many of the coastal stations that showed no effect on Day +0.5 have a pronounced effect on Day 1.5. All seven stations that show a statistically significant correlation on Day 1.5 are in the western end of the domain, and have correlations with r^2 ranging from 0.31–0.55. Another observation is that the downwind stations in the eastern side of the domain show a reduced effect on Day 1.5 compared to Day 0.5. This suggests that a different mechanism is likely responsible for the positive values of $dO_3/d\int[N_2O_5]dt$ on Day 1.5 compared to Day 0.5. Since there is little effect on Day 0.5 for coastal stations, and the marine air laden with overnight products is carried east into the valley on that day, it would suggest that an effect on Day 1.5 can only be seen at the coast if the air is transported back down the valley. This could be accomplished by a day time sea breeze circulation in an elevated layer, or a land breeze circulation at night in the surface layer. In either case, the effect is likely a transport effect, whereby high concentrations of photochemical products including O_3 from the previous day, are transported back to the coast. It is possible that ozone and other products are present in a residual layer that mixes downward upon inversion breakup, contributing to enhanced O_3 formation at the coastal stations on Day 1.5. The reduced value of $dO_3/d\int[N_2O_5]\,dt$ at the eastern downwind stations on Day 1.5 indicates the first sign of a dampening of the effect, which disappears altogether on Day 2.5 (see Fig. 11).

It should be noted here that while our observation of a correlation between overnight N_2O_5 and increased O_3 in the valley is consistent with a mechanism linked to the production of chlorine containing photolabile species, it is not proof that such a mechanism is operating. There are other plausible reasons that such a correlation may exist. Firstly, it is possible that other chemical species are involved. For example, increased production of HONO on nights with high N_2O_5 would produce a similar effect, as HONO is known to be an early morning source of OH. Other meteorological effects could also be responsible for such a correlation. For example, regional stagnation associated with high pressure systems could result in increased NO_x and N_2O_5 in the marine boundary layer overnight while simultaneously producing increased ozone on a regional scale. We cannot disprove such mechanisms in the current study. In future, measurements of photolabile species in the region as well as photochemical modelling efforts will be necessary in order to investigate the relative importance of all such effects, and ultimately to determine the role of chlorine-containing photolabile species in production of O_3 in polluted marine environments.

5 Conclusions

We report measurements of NO_3, NO_2, O_3 and calculated values of N_2O_5 in the polluted MBL. Median overnight levels of NO_2, NO_3 and N_2O_5 were 8.3 ppb, 10.2 ppt and 122 ppt, respectively. The range of NO_2, NO_3 and N_2O_5 levels were within the range of other reports in the moderately

polluted MBL, although the study median and average overnight levels of NO_2 and N_2O_5 are higher than other studies, indicative of high NO_2. Despite this, the median and average levels of NO_3 were similar to other moderately polluted MBLs, an indication of the dependence of both NO_3 formation and loss to form N_2O_5, on the amount of NO_2. The median and average values of the N_2O_5/NO_3 ratio were 13.1 and 16.8 respectively, much higher than seen in the clean MBL. Although this would lead to an expectation that losses in the N_2O_5/NO_3 reservoir would be dominated by losses of N_2O_5, we estimate that direct and indirect losses of NO_3 in the nocturnal reservoir are about equal. Our results also suggest there are reactive VOCs in the polluted MBL in this region, although further ancillary measurements of VOCs would be needed to support this suggestion.

We have used the argument that fast turnover times of NO_3 and N_2O_5 ensure that equilibrium is maintained in the $NO_2/NO_3/N_2O_5$ system due to warm overnight temperatures. The steady-state assumption could not be assumed however, due to high levels of NO_2. Non steady-state lifetimes of NO_3 were calculated using an expression that incorporates the derivatives $d[NO_3]/dt$ and $d[N_2O_5]/dt$. The non steady-state lifetimes of NO_3 were compared to steady-state lifetimes calculated using the common methodology. In general, there are differences such that steady-state lifetimes underestimate the true lifetime in the early parts of the night when the nocturnal reservoir is increasing, while the reverse is true in the latter parts of the night when N_2O_5 and NO_3 are depleting. Despite this, the overall distribution of NO_3 lifetimes observed throughout the study are somewhat similar, with median and average lifetimes in the range of 1.1–2.3 min. This should not be taken as a general observation though. The approach we have outlined here for calculating non steady-state lifetimes would be ideally suited for high temporal resolution measurements of NO_3 and N_2O_5 in polluted regions via new instrumental methods such as cavity ringdown spectroscopy.

The use of non steady-state lifetimes of NO_3, adds confidence to our method for the determination of losses from the nocturnal reservoir as a function of time during the night, especially the separate determination of the direct and indirect loss coefficients, k_x and k_y respectively. Our results show that direct losses of NO_3, likely through reactions with VOC's, are high early in the night, dropping off significantly as the night proceeds and consistent with a depletion of reactive VOCs in the MBL. It is unlikely that DMS can account for all these losses based on reported fluxes of DMS in the region. The magnitude of the loss coefficient for N_2O_5, k_y, is roughly consistent with recommended rates for the homogeneous reaction of H_2O with N_2O_5 early in the night, although it could also be a heterogeneous loss. Values of k_y rise in the latter part of the night, roughly coincident in time with an increase in the relative humidity past the deliquescence relative humidity of sea salt. The increase in k_y with increase in relative humidity is consistent with increased loss of N_2O_5 via heterogeneous reactions on deliquesced aerosols. The highest levels of the observational rate constant that we attribute to reaction of N_2O_5 on aerosols are in the range, $k_{het} = (1.2 \pm 0.4) \times 10^{-3}\,s^{-1} - (1.6 \pm 0.4) \times 10^{-3}\,s^{-1}$, (excluding or including homogeneous loss component, respectively), consistent with other recent reports for heterogeneous loss of N_2O_5 in the marine boundary layer.

Using a semi-observational approach, we find evidence for a link between nighttime chemistry in the marine boundary layer and ozone formation in the Lower Fraser Valley. Correlations between overnight integrated N_2O_5 measured at Saturna Island, and maximum 1-h ozone measured at stations in the Lower Fraser Valley the next day, were computed for a data set that only included nights when the next day showed a definitive sea breeze indicating transport of marine air into the valley as determined by observations at six meteorological stations within the valley. To rule out the possibility of a random link in the correlations, the correlations were also calculated for the maximum ozone on the two days preceding, and the two days following the day after a nighttime accumulation. The analysis indicated that there are statistically significant positive correlations between integrated N_2O_5 at Saturna and maximum 1-h ozone only on the two days following the nighttime accumulation. Positive correlations were non existent on the other three days. The magnitude of the average valley wide correlation on the day after (Day +0.5) was $d[O_3]/d\int[N_2O_5]dt = 18.8 \pm 4.8$ ppb$O_3 \times$ppb $N_2O_5^{-1}$ night^{-1}, which corresponds to an increase in peak ozone, $\Delta O_3 = +1.1$ ppb to $+8.3$ ppb, when we take into account the range of overnight integrals that were observed during the study

The spatial pattern of the correlations is presented for each day and appears to be different. On the day after (Day +0.5), insignificant effects were seen at stations closest to the coast in urban areas of Vancouver, while the largest effects, up to 50 ppb $O_3 \times$ppb $N_2O_5^{-1}$ night^{-1}, were seen at stations far down the valley. On the next day (Day +1.5), the coastal stations showed statistically significant effects while the correlations at the downwind stations were reduced. We interpret the above spatial effects as evidence of transport of marine air down the valley on the day after (Day +0.5), with increased chemical amplification in ΔO_3 as transport time increases. The mechanism responsible for the increased O_3 may include the photolysis of photolabile species that accumulate overnight to produce Cl, which contributes to enhanced photochemical ozone formation via VOC oxidation, although other mechanisms are possible. The mechanism of the second day (Day +1.5) is likely related to transport of polluted air back to the coast. The exact mechanism on the second day is not known, but it is plausible that it involves downward mixing of air in a residual layer that contains elevated O_3 and other precursors left over from the previous day.

While we see evidence for a correlation between nighttime chemistry in the marine boundary layer and maximum ozone in the valley, our analysis does not provide definitive proof that photolabile species are causing the effect. Further measurements of photolabile chlorine species in this or similar polluted marine environments and/or other evidence of Cl radicals being involved in the oxidation of VOCs would be needed to confirm this.

Acknowledgements. The authors acknowledge funding from the National Science and Engineering Research Council of Canada. We thank Al Percival of Metro Vancouver (formerly GVRD) for providing air quality data from the network. We thank Jason O'Brien and CAPMon/Environment Canada for providing data from the Saturna Island CAPMon station. We thank the lighthouse keepers, Roy and Marie Barrows for their hospitality and Carol Weldon for assistance in editing the manuscript.

Edited by: T. Bertram

References

Allan, B. J., McFiggans, G., Plane, J. M., Coe, H., and McFayden, G. G.: The nitrate radical in the remote marine boundary layer, J. Geophys. Res., 105, 24191–24204, 2000.

Ambrose, J. L., Mao, H., Mayne, H. R., Stutz, J., Talbot, R., and Sive, B. C.: Nighttime nitrate radical chemistry at Appledore Island, Maine during the 2004 International Consortium for Atmospheric Research on Transport and Transformation, , J. Geophys. Res., 112, D21302, doi:10.1029/2007JD008756, 2007.

Anlauf, K. G., Li, S.-M., Leaitch, R., Brook, J., Hayden, K. L., Toom-Sauntry, D., and Wiebe, A.: Ionic composition and size characteristics of particles in the Lower Fraser Valley: pacific 2001 field study, Atmos. Environ., 40, 2662–2675, 2006.

Atkinson, R., Baulch, D. L., Cox, R. A., Crowley, J. N., Hampson, R. F., Hynes, R. G., Jenkin, M. E., Rossi, M. J., and Troe, J.: Evaluated kinetic and photochemical data for atmospheric chemistry: Volume I – gas phase reactions of O_x, HO_x, NO_x and SO_x species, Atmos. Chem. Phys., 4, 1461–1738, 2004, http://www.atmos-chem-phys.net/4/1461/2004/.

Atkinson, R., Baulch, D. L., Cox, R. A., Crowley, J. N., Hampson, R. F., Hynes, R. G., Jenkin, M. E., Rossi, M. J., Troe, J., and IUPAC Subcommittee: Evaluated kinetic and photochemical data for atmospheric chemistry: Volume II – gas phase reactions of organic species, Atmos. Chem. Phys., 6, 3625–4055, 2006, http://www.atmos-chem-phys.net/6/3625/2006/.

Bogumil, K., Orphal, J., Burrows, J. P., and Flaud, J. M.: Vibrational progressions in the visible and near-ultraviolet absorption spectrum of ozone, Chem. Phys. Lett., 349, 241–248, 2001.

Brook, J. R., Strawbridge, K. B., Snyder, B. J., Boudries, H., Worsnop, D., Sharma, S., Anlauf, K. G., and Hayden, K. L.: Towards an understanding of the fine particle variations in the LFV: integration of chemical, physical and meteorological observations, Atmos. Environ., 38 , 5775–5788, 2004.

Brown, S. S., deGouw, J. A., Warneke, C., Ryerson, T. B., Dub, W. P., Atlas, E., Weber, R. J., Peltier, R. E., Neuman, J. A., Roberts, J. M., Swanson, A., Flocke, F., McKeen, S. A., Brioude, J., Sommariva, R., Trainer, M., Fehsenfeld, F. C., and Ravishankara, A. R.: Nocturnal isoprene oxidation over the Northeast United States in summer and its impact on reactive nitrogen partitioning and secondary organic aerosol, Atmos. Chem. Phys., 9, 3027–3042, 2009, http://www.atmos-chem-phys.net/9/3027/2009/.

Brown, S. S., Dibb, J. E., Stark, H., Aldener, M., Vozella, M., Whitlow, S., Williams, E. J., Lerner, B. M., Jakoubek, R., Middlebrook, A. M., DeGouw, J. A., Warneke, C., Goldan, P. D., Kuster, W. C., Angevine, W. M., Sueper, D. T., Quinn, P. K., Bates, T. S., Meagher, J., Fehsenfeld, F. C., and Ravishankara, A. R.: Nighttime removal of NO_x in the summer marine boundary layer, Geophys. Res. Lett., 32, L07108, doi:10.1029/2004GL019412, 2004.

Brown, S. S., Dubé, W. P., Fuchs, H., Ryerson, T. B., Wollny, A. G., Brock, C. A., Bahreini, R., Middlebrook, A. M., Neuman, J. A., Atlas, E., Roberts, J. M., Osthoff, H. D., Trainer, M., Fehsenfeld, F. C., and Ravishankara, A. R.: Reactive uptake coefficients for N_2O_5 determined from aircraft measurements during the Second Texas Air Quality Study: Comparison to current model parameterizations, J. Geophys. Res., 114, D00F10, doi:10.1029/2008JD011679, 2009.

Brown, S. S., Dubé, W. P., Osthoff, H. D., Wolfe, D. E., Angevine, W. M., and Ravishankara, A. R.: High resolution vertical distributions of NO_3 and N2O5 through the nocturnal boundary layer, Atmos. Chem. Phys., 7, 139–149, 2007, http://www.atmos-chem-phys.net/7/139/2007/.

Brown, S. S., Stark, H., and Ravishankara, A. R.: Applicability of the steady state approximation to the interpretation of atmospheric observations of NO_3 and N_2O_5, J. Geophys. Res., 108(D17), 4539, doi:10.1029/2003JD003407, 2003a.

Brown, S. S., Stark, H., Ryerson, T. B., and et al.: Nitrogen oxides in the nocturnal boundary layer: simultaneous, in-situ detection of NO_3 , N_2O_5, NO, NO_2 and O_3, J. Geophys. Res., 108, 4299 doi:10.1029/2002JD002917, 2003b.

Coheur, P. F., Fally, S., Carleer, M., Clerbaux, C., Colin, R., Jenouvrier, A., Mérienne, M.-F., Hermans, C., and Vandaele, A. C.: New water vapor line parameters in the 26000–13000 cm^{-1} region, J. Quant. Spectrosc. Radiat. Transfer, 74, 493–510, 2002.

Dentener, F. J. and Crutzen, P. J.: Reaction of N_2O_5 on tropospheric aerosols: impact on the global distributions of NO_x, O_3, and OH, J. Geophys. Res., 98, 7149–7163, 1993.

Dimitroulopoulou, C. and Marsh, A. R. W.: Modelling studies of NO_3 nighttime chemistry and its effects on subsequent ozone formation, Atmos. Environ., 31, 3041–3057, 1997.

Environment Canada, National Climate Data and Information Archive. http://www.climate.weatheroffice.ec.gc.ca/Welcome_e.html, 2008.

Finlayson-Pitts, B. J.: The tropospheric chemistry of sea salt: a molecular-level view of the chemistry of NaCl and NaBr, Chemical Reviews, 103, 4801–4822, 2003.

Finlayson-Pitts, B. J., Ezell, M. J., and Pitts Jr., J. N.: Formation of chemically active chlorine compounds by reactions of atmospheric NaCl particles with gaseous N_2O_5 and $ClONO_2$, Nature, 337, 241–244, 1989.

Finlayson-Pitts, B. J. and Pitts Jr., J. N.: Chemistry of the Upper and Lower Atmosphere, Academic Press, San Diego, 2000.

Finley, B. D. and Saltzman, E. S.: Measurement of Cl_2 in coastal urban air, Geophys. Res. Lett., 33, L11809, doi:10.1029/2006GL025799, 2006.

Fuchs, N. A. and Sutugin, A. G., High dispersed aerosols, Int. Rev.

Aer. Phys. Chem., 2, 1–60, 1971.

Geyer, A., Alicke, B., Konrad, S., Schmitz, T., Stutz, J., and Platt, U., Chemistry and oxidation capacity of the nitrate radical in the continental boundary layer near Berlin, J. Geophys. Res., 106, 8013–8025, 2001.

Hedley, M., McLaren, R., Jiang, W., and Singleton, D. L.: Evaluation of an air quality simulation of the Lower Fraser Valley. Part II: photochemistry, Atmos. Environ., 31, 1617–1630, 1997a.

Hedley, M. and Singleton, D. L.: Evaluation of an air quality simulation of the Lower Fraser Valley-1. Meteorology, Atmos. Environ., 31, 1605–1615, 1997b.

Hedley, M., Jiang, W., McLaren, R., and Singleton, D. L.: Modelling of future year emissions control scenarios for the Lower Fraser Valley: impacts of natural gas and propane vehicle technologies, J. App. Met., 37, 1190–1204, 1998.

Heintz, F., Platt, U., Flentje, H., and Dubois, R.: Long-term observation of nitrate radicals at the Tor station, Kap Arkona (Rügen), J. Geophys. Res., 101, 22891–22910, 1996.

Jiang, W., Singleton, D. L., Hedley, M., and McLaren, R.: Comparison of organic compound compositions in the emissions inventory and ambient data for the Lower Fraser Valley, J. Air and Waste Manag. Assoc., 47, 851–860, 1997.

Knipping, E. M., Lakin, M. J., Foster, K. L., Jungwirth, P., Tobias, D. J., Gerber, R. B., Dabdub, D., and Finlayson-Pitts, B. J.: Experiments and simulations of ion-enhanced interfacial chemistry on aqueous NaCl aerosols , Science, 288, 301–306, 2000.

Knipping, E. M. and Dabdub, D.: Environmental Science and Technology, 37, 275–284, 2003.

Kraus, S. G.: DOASIS: A framework design for DOAS,thesis, Universität Mannheim, Germany , 2006.

Li, S.-M.: A concerted effort to understand the ambient particulate matter in the Lower Fraser Valley: the Pacific 2001 air quality study, Atmos. Environ., 38, 5719–5731, 2004.

Lu, G., Brook, J., Alfarra, M. R., Anlauf, K. G., Leaitch, W. R., Sharma, S., Wang, D., Worsnop, D. R., and Phinney, L.: Identification and characterization of inland ship plumes over Vancouver, BC, Atmos. Environ., 40, 2767–2782, 2006.

Martinez, M., Perner Dieter, Hackenthal, E.-M., Külzer, S., and Schütz, L.: NO_3 at Helgoland during the NORDEX campaign in October 1996, J. Geophys. Res., 105, 22685–22695, 2000.

Matsumoto, J., Imagawa, K., Imai, H., Kosugi, N., Ideguchi, M., Kato, S., and Kajii, Y., Nocturnal sink of NO_x via NO_3 and N_2O_5 in the outflow from a source area in Japan, Atmos. Environ., 40, 6294–6302, 2006.

McLaren, R., Salmon, R. A., Liggio, J., Hayden, K. L., Anlauf, K. G., and Leaitch, W. R., Nighttime chemistry at a rural site in the Lower Fraser Valley, Atmos. Environ., 38, 5837–5848, 2004.

Metro Vancouver, Lower Fraser Valley Air Emissions Inventory and Forecast and Backcast. 2007. Burnaby, BC, Metro Vancouver Policy and Planning Department, Air Quality Policy and Management Division, 2005.

Noxon, J. F., Norton, R. B., and Marovich, E.: NO_3 in the troposphere, Geophys. Res. Lett., 7, 125–128, 1980.

Orlando, J. J., Tyndall, G. S., Moortgat, G. K., and Calvert, J. G.: Quantum Yields for NO_3 photolysis between 570 and 635 nm, J. Chem. Phys., 97, 10996–11000, 1993.

Osthoff, H. D., Pilling, M. J., Ravishankara, A. R., and Brown, S. S.: Temperature dependence of the NO_3 absorption cross-section above 298 K and determination of the equilibrium constant for NO_3+NO_2 $\leftrightarrow$$2N_2O_5$ at atmospherically relevant conditions, Phys. Chem. Chem. Phys., 9, 5785–5793, 2007.

Osthoff, H. D., Roberts, J. M., Ravishankara, A. R., Williams, E. J., Lerner, B. M., Sommariva, R., Bates, T. S., Coffman, D., Quinn, P. K., Dibb, J. E., Stark, H., Burkholder, J. B., Talukdar, R. K., Meagher, J., Fehsenfeld, F. C., and Brown, S. S.: High levels of nitryl chloride in the polluted subtropical marine boundary layer, Nature Geoscience, 1, doi:10.1038/ngeo177, 324–328, 2008.

Platt, U.: Differential optical absorption spectroscopy (DOAS), in Air monitoring by spectroscopic techniques, edited by: Sigrist, M. W., 27–84, John Wiley and Sons, Inc., Toronto, 1994.

Platt, U., Perner Dieter, Winer, A. M., Harris, G. W., and Pitts Jr., J. N., Detection of NO_3 in the polluted troposphere by differential optical absorption, Geophys. Res. Lett., 7, 89–92, 1980.

Raff, J. D., Njegic, B., Chang, W. L., Gordon, M. S., Dabdub, D., Gerber, R. B., and Finlayson-Pitts, B. J.: Chlorine activation indoors and outdoors via surface-mediated reactions of nitrogen oxides with hydrogen chloride, Proc. Natl. Acad. Sci. USA, 106, 13647–13654, 2009.

Roberts, J. M., Osthoff, H. D., Brown, S. S., and Ravishankara, A. R.: N_2O_5 oxidizes chloride to Cl_2 in acidic atmospheric aerosol, Science, 321, p. 1059, 2008.

Seinfeld, J. H. and Pandis, S. N.: Atmospheric Chemistry and Physics: from air pollution to climate change, Wiley-Interscience, New Jersey, USA, 2006.

Sharma, S., Vingarzan, R., Barrie, L. A., Norman, A., Sirois, A., Henry, M., and DiCenzo, C.: Concentrations of dimethyl sulfide in the Strait of Georgia and its impact on the atmospheric sulfur budget of the Canadian West Coast J. Geophys. Res., 108, 4459, doi:10.1029/2002JD002447, 2003.

Simon, H., Kimura, Y., McGaughey, G., Allen, D. T., Brown, S. S., Osthoff, H. D., Roberts, J. M., Byun, D., and Lee, D.: Modeling the impact of $ClNO_2$ on ozone formation in the Huston area , J. Geophys. Res., 114, D00F03, doi:10.1029/2008JD010732, 2009.

Snyder, B. J. and Strawbridge, K. B.: Meteorological analysis of the Pacific 2001 air quality field study, Atmos. Environ., 38, 5733–5743, 2004.

Spicer, C. W., Chapman, E. G., Finlayson-Pitts, B. J., Plastridge, R. A., Hubbe, J. M., Fast, J. D., Berkowitz, C. M., Vrekoussis, M., Kanakidou, M., Mihalopoulos, N., Crutzen, P. J., Lelieveld, J., Perner, D., Beresheim, H., and Baboukas, E.: Unexpectedly high concentrations of molecular chlorine in coastal areas, Nature, 394, 353–356, 1998.

Steyn, D. G., Bottenheim, J. W., and Thomson, R. B.: Overview of tropospheric ozone in the Lower Fraser Valley: the Pacific '93 field study, Atmos. Environ., 31, 2025–2036, 1997.

Stutz, J. and Platt, U.: Improving long-path differential optical absorption spectroscopy with a quartz-fiber mode mixer, App. Opt., 36, 1105–1115, 1997.

Tang, I. N., Tridico, A. C., and Fung, K. H., Thermodynamic and optical properties of sea salt aerosols, J. Geophys. Res., 102, 23269–23275, 1997.

Voigt, S., Orphal, J., and Burrows, J. P.: The temperature and pressure dependence of the absorption cross-sections of NO_2 in the 250–800 nm region measured by Fourier-transform spectroscopy, J. Photochem. Photobiol. Chem., 149, 1–7, 2002.

Vrekoussis, M., Kanakidou, M., Mihalopoulos, N., Crutzen, P. J., Lelieveld, J., Perner, D., Berresheim, H., and Baboukas, E.: Role

of the NO_3 radicals in oxidation processes in the eastern Mediterranean troposphere during the MINOS campaign, Atmos. Chem. Phys., 4, 169–182, 2004, http://www.atmos-chem-phys.net/4/169/2004/.

Vrekoussis, M., Mihalopoulos, N., Gerasopoulos, E., Kanakidou, M., Crutzen, P. J., and Lelieveld, J.: Two-years of NO_3 radical observations in the boundary layer over the Eastern Mediterranean, Atmos. Chem. Phys., 7, 315–327, 2007, http://www.atmos-chem-phys.net/7/315/2007/.

Wahner, A., Mentel, Th. F., and Sohn, M.: Gas-phase reaction of N_2O_5 with water vapor:Importance of heterogeneous hydrolysis of N_2O_5 and surface desorption of HNO_3 in a large teflon chamber, Geophys. Res. Lett., 25, 2169–2172, 1998.

Wängberg, I., Barnes, I., and Becker, K. H.: Product and mechanistic study of the reaction of NO_3 radicals with α-pinene, Environ. Sci. Technol., 31, 2130–2135, 1997.

Wängberg, I., Etzkorn, T., Barnes, I., Platt, U., and Becker, K. H.: Absolute determination of the temperature behaviour of the NO_2+NO_3+(M)↔N_2O_5+(M) equilibrium., J. Phys. Chem., 101, 9694–9698, 1997.

Yokelson, R. J., Burkholder, J. B., Fox, R. W., Talukdar, R. K., and Ravishankara, A. R.: Temperature dependence of the NO_3 absorption spectrum, J. Phys. Chem., 98, 13144–13150, 1994.